3D to 2D approximation effect on propagation modeling, impact on scintillation indices

<u>V. Fabbro[1]</u>, L. Féral[2], H. Galiegue[3] and S. Rougerie[4]

[1] DEMR, ONERA, 2 avenue Edouard Belin, Toulouse, FRANCE.
[2] Laboratoire LAPLACE, GRE, Université Paul Sabatier, Toulouse, FRANCE.
[3] TELECOM-EMA, ENAC, 7 avenue Edouard Belin, Toulouse, FRANCE. .
[4]CNES, 18 avenue Edouard Belin, Toulouse, FRANCE. .

Beacon Satellite Symposium 2016

Dimensional reduction issues

Modeling of transionospheric propagation with numerical schemes:

3D configuration

☺ Full description of the turbulent medium

☹ Numerical run can take a long time

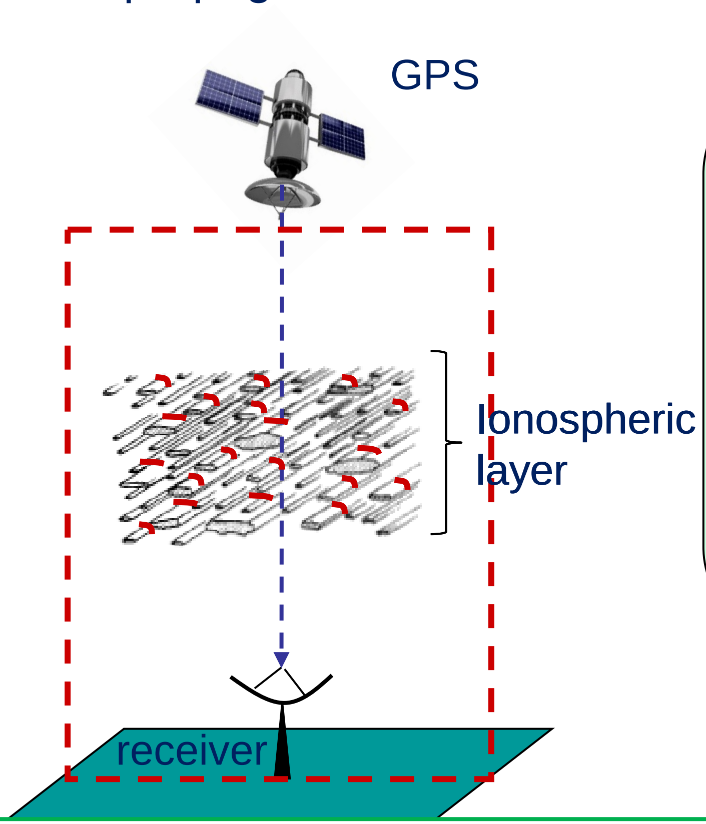

2D configuration

☺Faster computation time

☹ Dimensional reduction of the turbulent medium

Errors potentially induced by the **dimensional reduction** have to be **quantitatively assessed from analytical derivations**

ONERA

3D to 2D approximation effect on propagation modeling, impact on scintillation indices

Content

- Propagation geometry and medium description
- 3D and 2D numerical schemes
- 3D and 2D analytical derivations
- Results in equatorial configuration
- Results in polar configuration
- Conclusions

3D to 2D approximation effect on propagation modeling, impact on scintillation indices

Content

- **Propagation geometry and medium description**
- 3D and 2D numerical schemes
- 3D and 2D analytical derivations
- Results in equatorial configuration
- Results in polar configuration
- Conclusions

Propagation geometry and medium description

Electron-density fluctuations are described by *Shkarofsky* [1968] spectrum:

$$S_{\Delta N_e}\left(K_{x_H}, K_{y_H}, K_{z_H}\right) = A_x A_y A_z C_s \left(A_x^2 K_{x_H}^2 + A_y^2 K_{y_H}^2 + A_z^2 K_{z_H}^2 + K_0^2\right)^{-p/2}$$

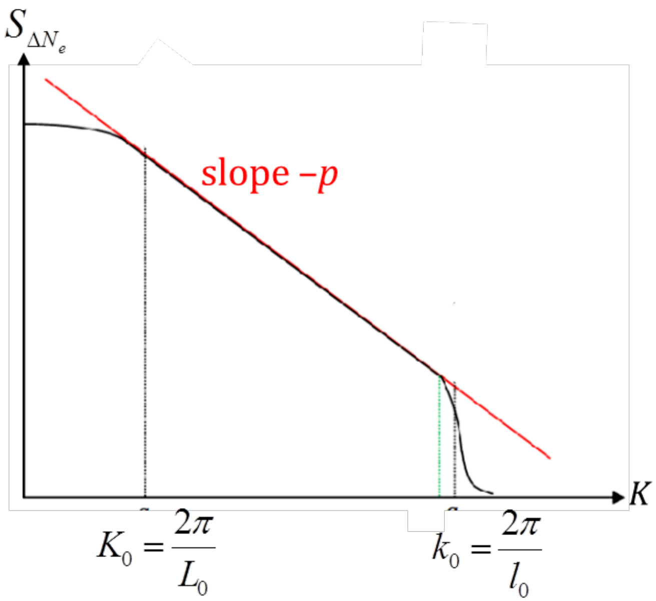

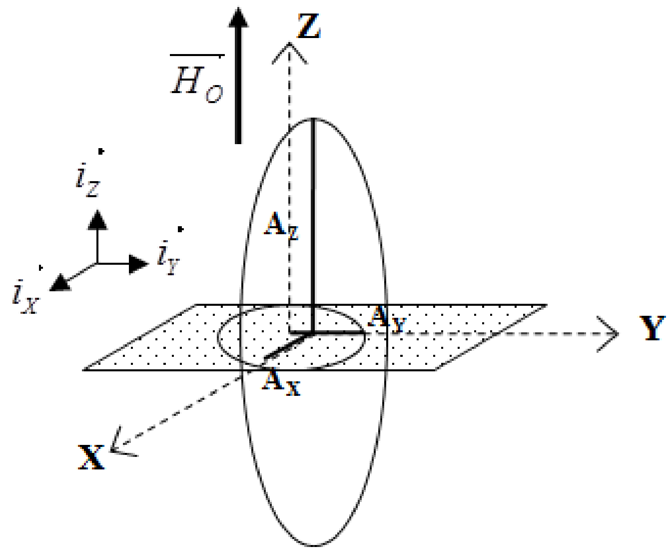

Fig.1: Spectrum of electron-density fluctuations

Fig.2: Ellipsoidal ionospheric irregularity With anisotropy ratios A_X=A_Y=1 and A_Z elongated along the terrestrial magnetic field H_0

Propagation geometry and medium description

LOS coordinate system (u, v, s) used to solve the Helmholtz scalar equation

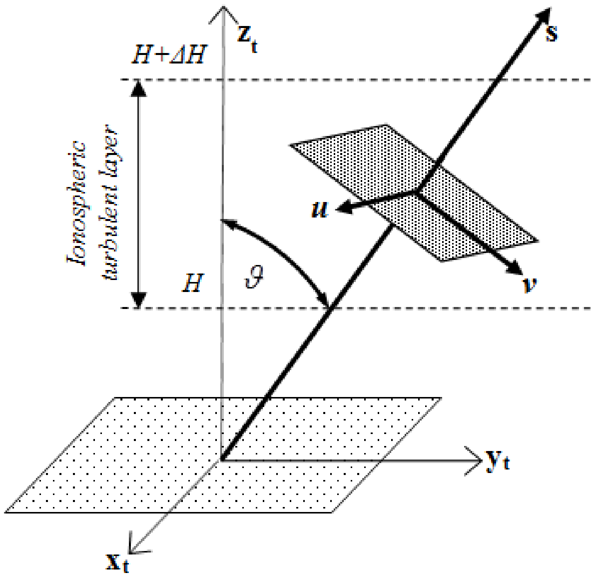

Fig.3: LOS coordinate system *(u,v,s)*

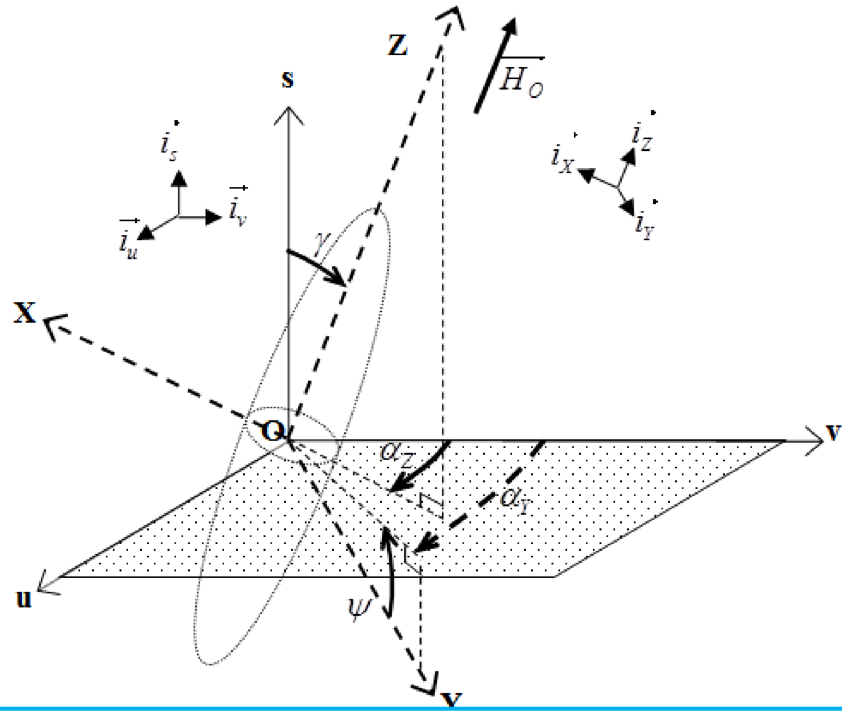

Fig.4: Geometry of the ionospheric turbulent Irregularities in the LOS coordinate system *(u,v,s)*

3D to 2D approximation effect on propagation modeling, impact on scintillation indices

Content

Parabolic Wave Equation Method with multiple Phase screen

Helmholtz equation resolution:

$$\boxed{\nabla^2 \underline{E}(\vec{r}) + k_o^2[1 + 2\Delta n(\vec{r}, t)]\underline{E}(\vec{r}) = 0}$$

Iterative Solution of PWE (Split-Step Fourier SSF) :

$$\underline{E}(u,v,s+\delta s) = e^{ik_o \boxed{\phi(u,v)}} \boxed{TF^{-1}\left\{ e^{i\sqrt{k_o^2 - K_u^2 - K_v^2}\,\delta s} TF[\underline{E}(u,v,s)] \right\}}$$

Propagation in vacuum

Phase Screen

$$\boxed{\phi(u,v) = \int_s^{s+\delta s} \Delta n(u,v,\xi)\, d\xi = -\frac{r_e \lambda}{k_o} \int_s^{s+\delta s} \Delta N_e(u,v,\xi)\, d\xi}$$

Propagation geometry and medium description

3D-PWE/2D-MPS

$$S_{\phi}^{2D}(K_u,K_v)=2\pi\left(\frac{r_e\lambda}{k_o}\right)^2\delta s\,S_{\Delta N_e}^{3D}(K_u,K_v,K_s=0)$$

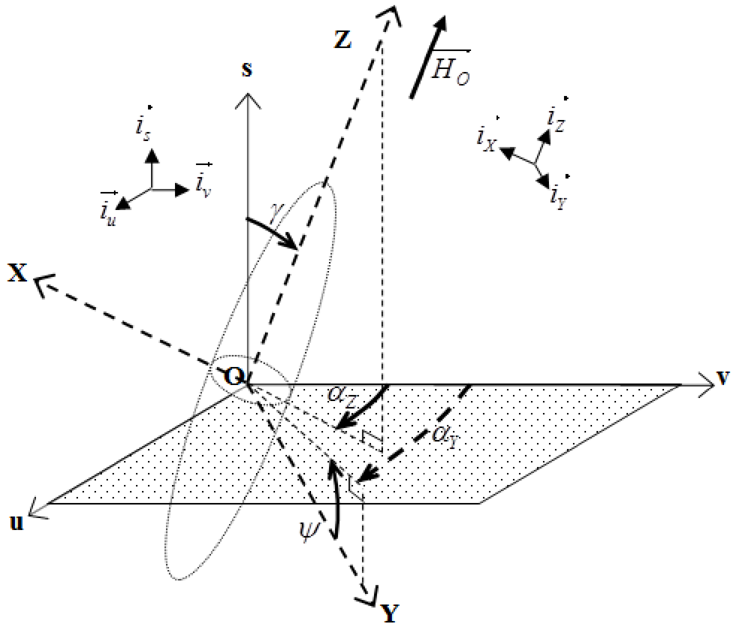

Fig.4: Geometry of the ionospheric turbulent Irregularities in the LOS coordinate system *(u,v,s)*

$$S_{\Delta N_e}^{3D}(K_u,K_v,K_s=0)=2\pi\left(\frac{r_e\lambda}{k_o}\right)^2\delta s\,a_X^{3-p}A_YA_ZC_S\left(AK_u^2+BK_v^2+2CK_uK_v+\frac{K_{os}^2}{a_X^2}\right)^{-p/2}$$

where

$$A=(\sin\gamma\cos\alpha_Z\sin\psi+\cos\alpha_Y\cos\psi\cos\gamma)^2+A_Y^2\sin^2\alpha_Y\cos^2\psi+A_Z^2\sin^2\gamma\sin^2\alpha_Z$$

$$B=(\cos\psi\sin\alpha_Y\cos\gamma+\sin\psi\sin\alpha_Z\sin\gamma)^2+A_Y^2\cos^2\psi\cos^2\alpha_Y+A_Z^2\sin^2\gamma\cos^2\alpha_Z$$

$$C=-(\sin\gamma\cos\alpha_Z\sin\psi+\cos\alpha_Y\cos\psi\cos\gamma)(\cos\psi\sin\alpha_Y\cos\gamma+\sin\psi\sin\alpha_Z\sin\gamma)$$
$$+A_Y^2\sin\alpha_Y\cos^2\psi\cos\alpha_Y+A_Z^2\sin\alpha_Z\sin^2\gamma\cos\alpha_Z$$

Coefficient formulations different of [Rino, 1979] because derived in LOS geometry

PWE-MPS Scheme

3D-PWE/2D-MPS

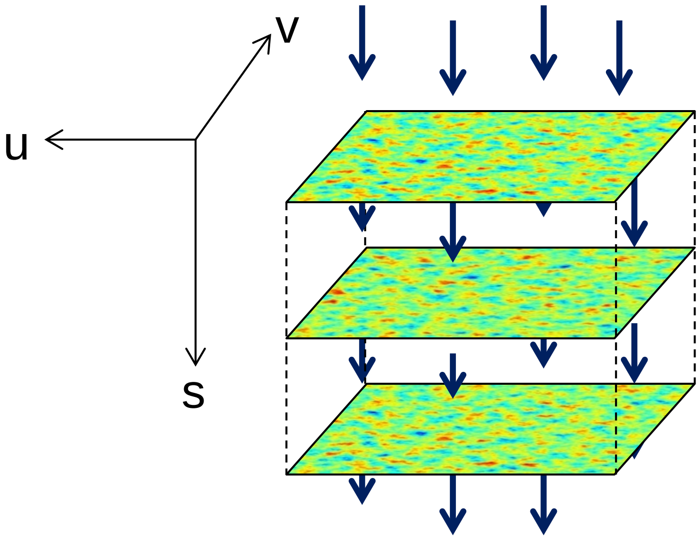

2D-PWE/1D-MPS

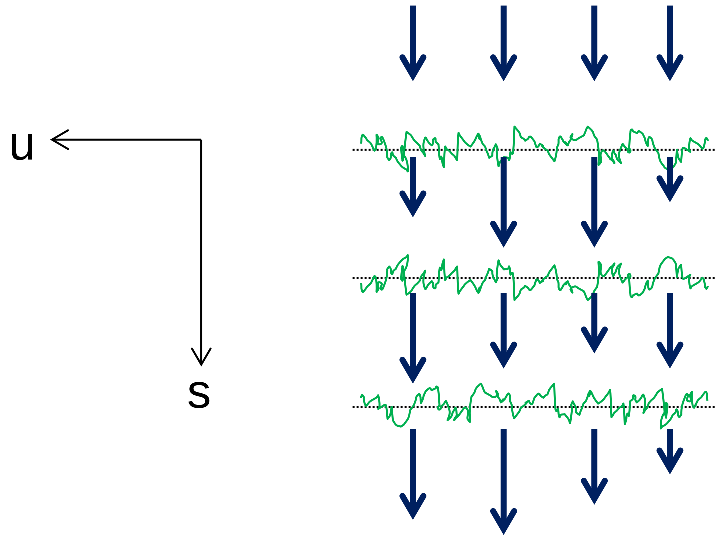

Reduced computation time

3D to 2D approximation effect on propagation modeling, impact on scintillation indices

Content

- Propagation geometry and medium description
- 3D and 2D numerical schemes
- **3D and 2D analytical derivations**
- Results in equatorial configuration
- Results in polar configuration
- Conclusions

Analytical derivations under weak scattering assumption

Analytical resolution of Helmholtz equation in stochastic medium:

$$\nabla^2 \underline{E}(\vec{r}) + k_o^2[1 + 2\Delta n(\vec{r},t)]\underline{E}(\vec{r}) = 0$$

Under weak scattering assumption [*Rytov et al.*, 1989]:

$$E(\vec{r}) = E_0(\vec{r})e^{\boxed{\Psi_1(\vec{r})}}$$

$$\Psi_1^{3D}(\vec{r}) = -2k_0^2 \iiint d^3 r G^{3D}\left(\vec{R},\vec{r}\right)\Delta n(\vec{r})\frac{E_0(\vec{r})}{E_0(\vec{R})}$$

$$\Psi_1^{2D}(\vec{r}) = -2k_0^2 \iint d^2 r G^{2D}\left(\vec{R},\vec{r}\right)\Delta n(\vec{r})\frac{E_0(\vec{r})}{E_0(\vec{R})}$$

variances (log-amplitude and phase) **are computed in LOS in 3D and 2D**

Analytical derivations under weak scattering assumption

For plane waves, the classical 3D expressions for log-amplitude variances [*Wheelon*, 2004b] are now given in the LOS by:

$$\langle \chi^2 \rangle^{3D} = (2\pi\lambda^2 r_e^2 \Delta H \sec\vartheta) \iint_{-\infty}^{+\infty} dK_u dK_v \, S_{\Delta N_e}^{3D}(K_u, K_v, 0) \, F_\chi^{3D}(K_u, K_v),$$

in 2D [Fabbro and Féral, 2012]:

$$\langle \chi^2 \rangle^{2D} = (2\pi\lambda^2 r_e^2 \Delta H \sec\vartheta) \iint_{-\infty}^{+\infty} dK_u dK_v \, S_{\Delta N_e}^{3D}(K_u, K_v, 0) \, F_\chi^{3D}(K_u, 0),$$

$F_\chi^{3D}(K_u, K_v)$ departs from 0 and crosses its asymptotic value 0.5 for the first time more rapidly than $F_\chi^{3D}(K_u, 0)$.

it follows that $\langle \chi^2 \rangle^{2D}$ is expected to be **lower** than $\langle \chi^2 \rangle^{3D}$

ONERA

Analytical derivations under weak scattering assumption

For plane waves, the classical 3D expressions for phase variances [*Wheelon*, 2004b] are now given in the LOS by:

$$\langle \varphi^2 \rangle^{3D} = (2\pi\lambda^2 r_e^2 \Delta H \sec\vartheta) \iint_{-\infty}^{+\infty} dK_u dK_v \, S_{\Delta N_e}^{3D}(K_u, K_v, 0) \, F_\varphi^{3D}(K_u, K_v)$$

in 2D [Fabbro and Féral, 2012]:

$$\langle \varphi^2 \rangle^{2D} = (2\pi\lambda^2 r_e^2 \Delta H \sec\vartheta) \iint_{-\infty}^{+\infty} dK_u dK_v \, S_{\Delta N_e}^{3D}(K_u, K_v, 0) \, F_\varphi^{3D}(K_u, 0)$$

since $F_\varphi^{3D}(K_u, K_v) = 1 - F_\chi^{3D}(K_u, K_v)$,

the reduction 3D/2D might lead to an **overestimation** of the phase variances

ONERA

Analytical derivations under weak scattering assumption

Analytical derivations :

in Fresnel regime and assuming that the thin-layer approximation $\Delta H \ll 2\,H$ holds:

$$\Re_\chi = \frac{<\chi^2>^{3\mathrm{D}}}{<\chi^2>^{2\mathrm{D}}}$$

$$= \frac{\pi}{2^{p-2}} \frac{\Gamma(p-1)}{\left[\Gamma(p/2-1/2)\right]^2} \left(\frac{A'}{B'}\right)^{(p-1)/2} \left[1+\left(\frac{A'}{B'}-1\right)\sin^2\varepsilon\right]^{1-p/2} {}_2F_1(p/2,1/2;1;1-A'/B')$$

$$\Re_\varphi = \frac{<\varphi^2>^{3\mathrm{D}}}{<\varphi^2>^{2\mathrm{D}}} = \frac{\Phi-\Re_\chi}{\Phi-1}$$

with

$$\Phi = \frac{a_X^{p-2}}{(2\sqrt{\pi})^{p-3}} \left(\frac{L_{os}}{\sqrt{\lambda H \sec\vartheta}}\right)^{p-2} \frac{\Gamma(p-1)\Gamma(p/4)}{\Gamma(3/2-p/4)\left[\Gamma(p/2-1/2)\right]^2} \left(\frac{A'\,B'}{B}\right)^{p/2-1}$$

3D to 2D approximation effect on propagation modeling, impact on scintillation indices

Content

- Propagation geometry and medium description
- 3D and 2D numerical schemes
- 3D and 2D analytical derivations
- **Results in equatorial configuration**
- Results in polar configuration
- Conclusions

Results in Equatorial configuration

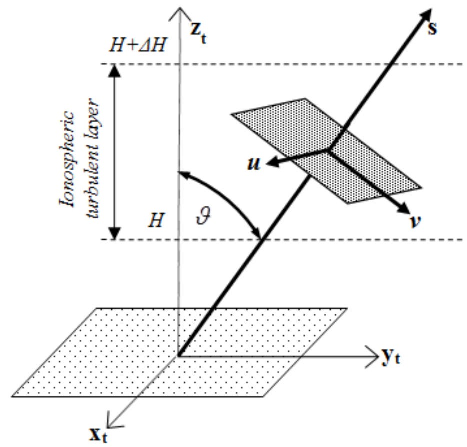

2 equatorial configurations considered:

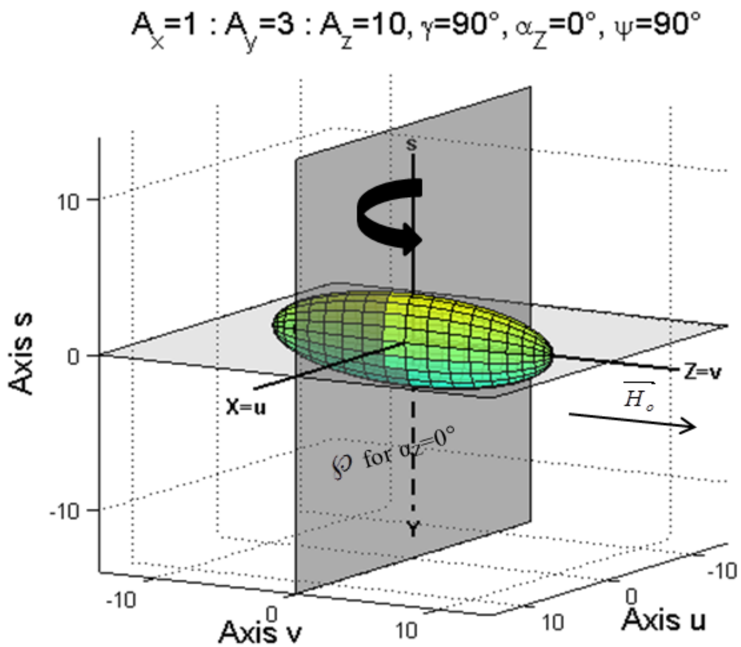

Fig.5: Ionospheric irregularity in the LOS coordinate system *(u,v,s)* for the 1st equatorial configuration

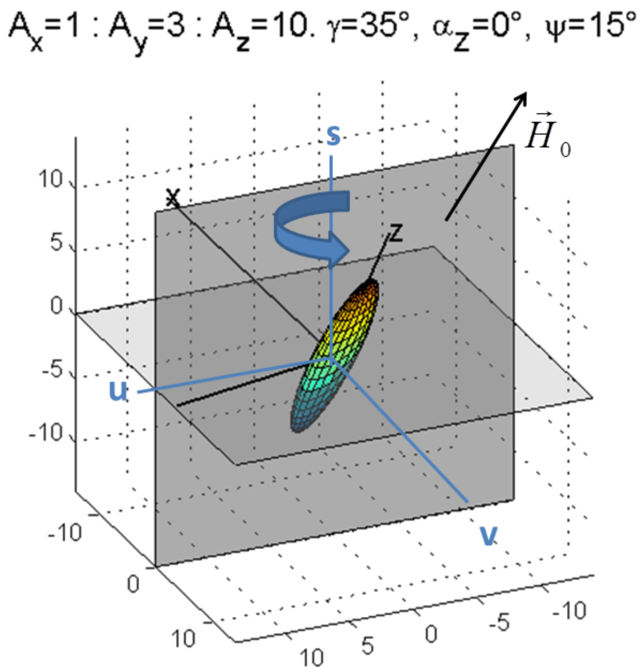

Fig.6: Ionospheric irregularity in the LOS coordinate system *(u,v,s)* for the 2nd equatorial configuration

ONERA

Results in Equatorial configuration

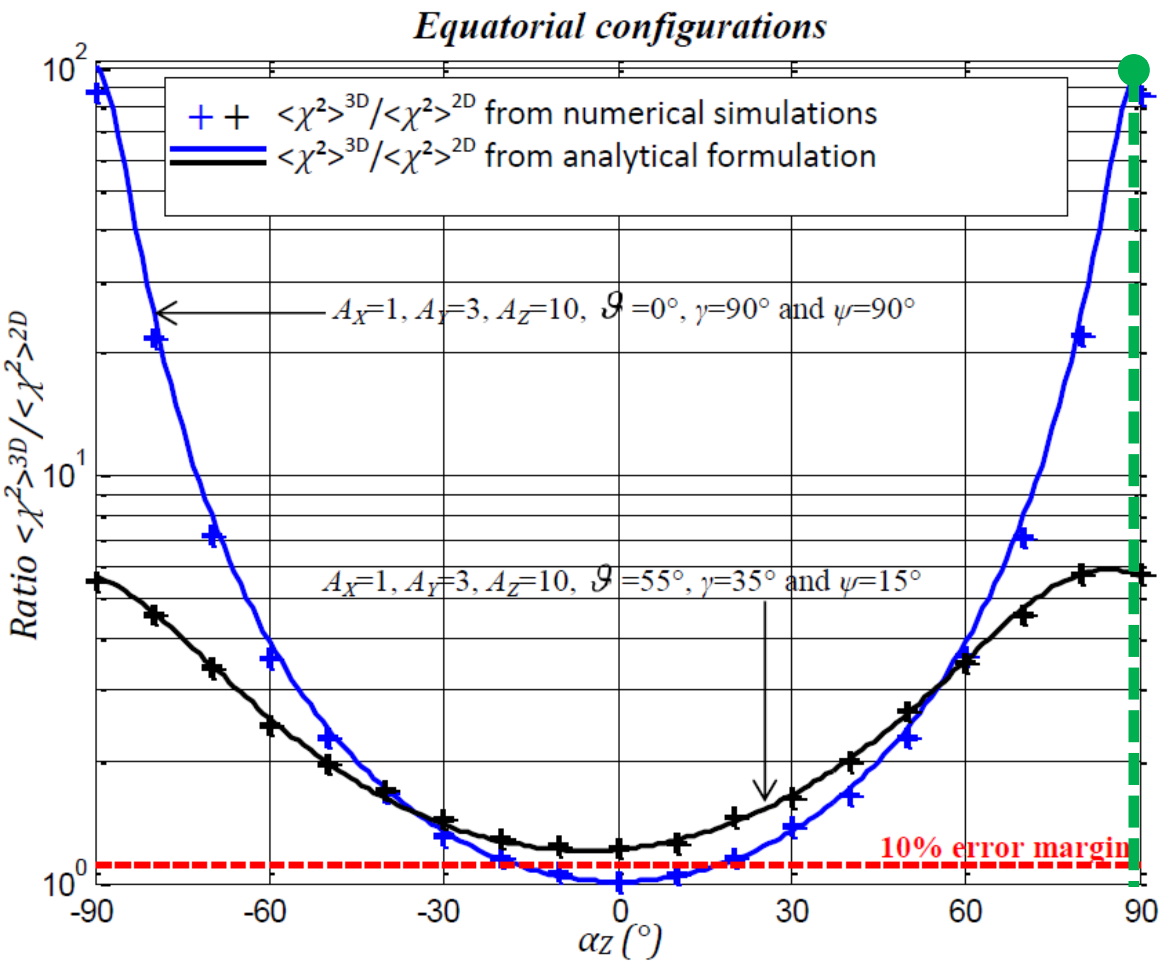

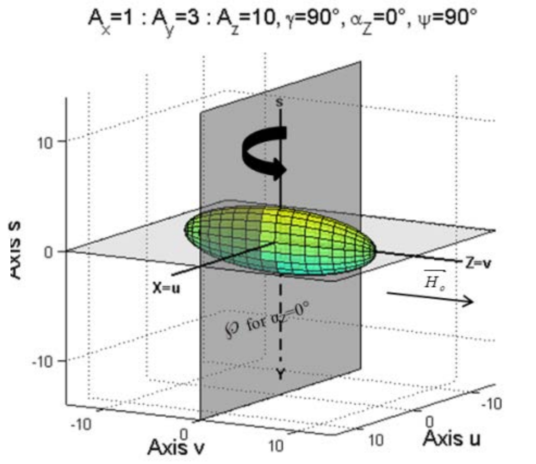

Top View (uOv)
(LOS transverse plane)

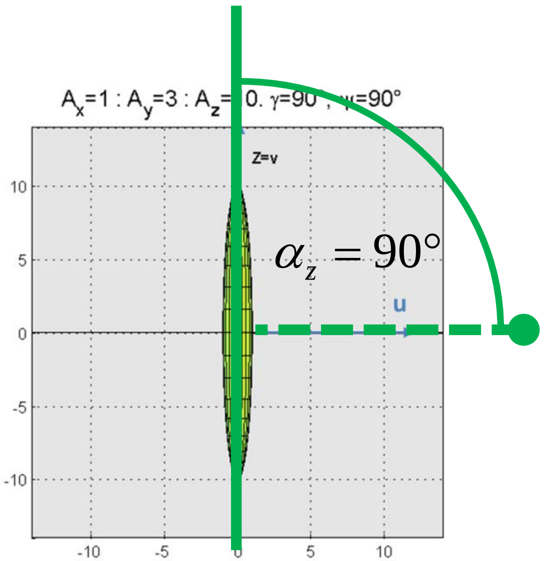

Fig.7: Ratio of log-amplitude variances derived from 3D and 2D numerical simulations (+) and analytical (-) as a function of the plane of dimensional reduction defined by α_Z

Results in Equatorial configuration

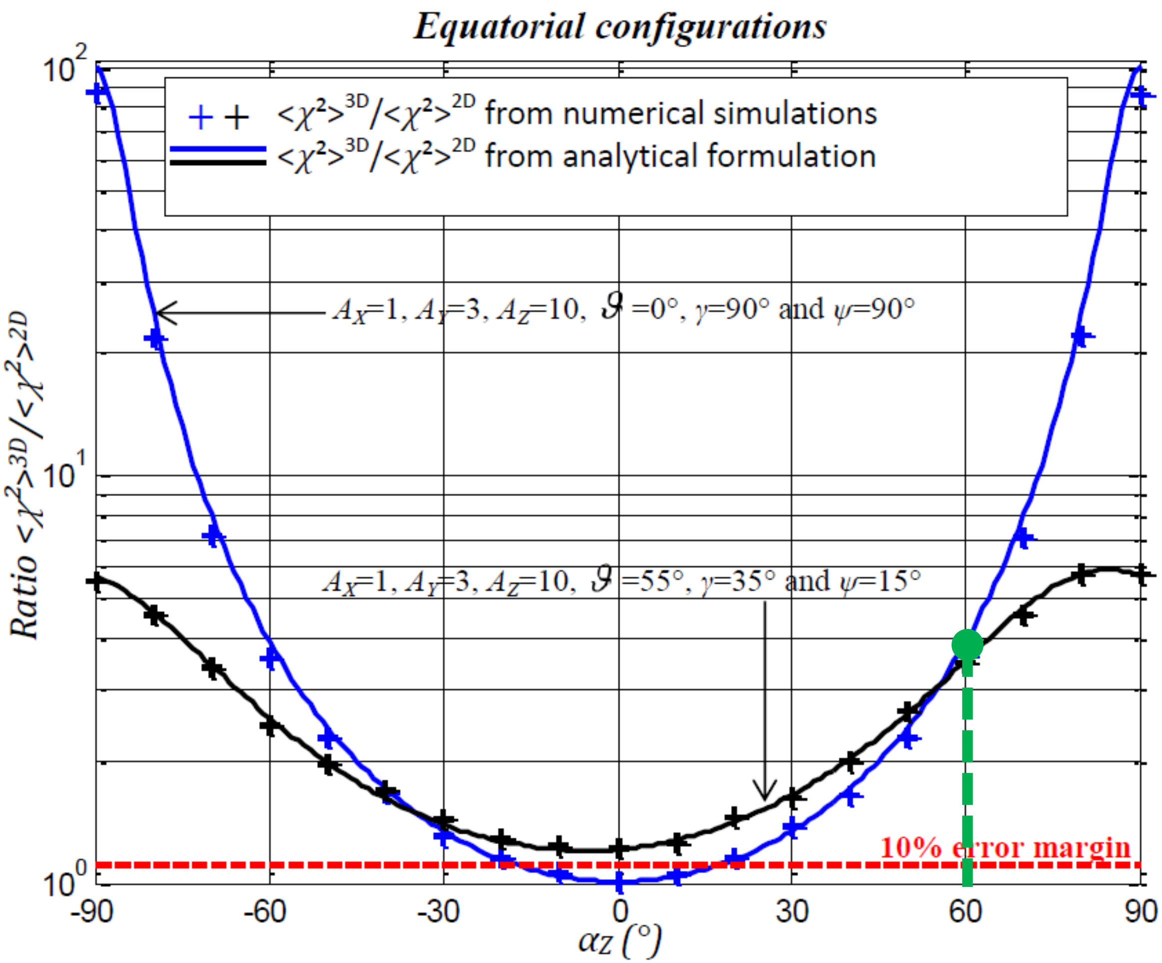

Fig.7: Ratio of log-amplitude variances derived from 3D and 2D numerical simulations (+) and analytical (-) as a function of the plane of dimensional reduction defined by α_Z

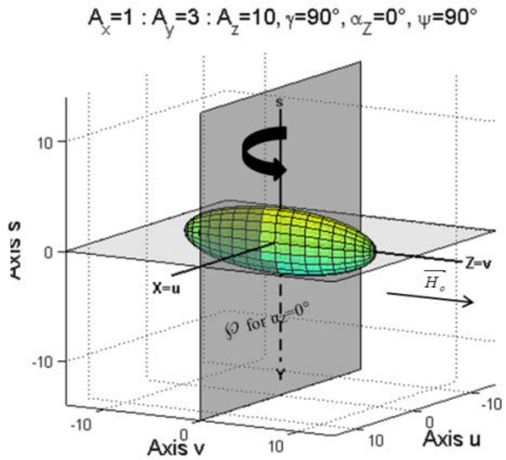

Top View (uOv)

(LOS transverse plane)

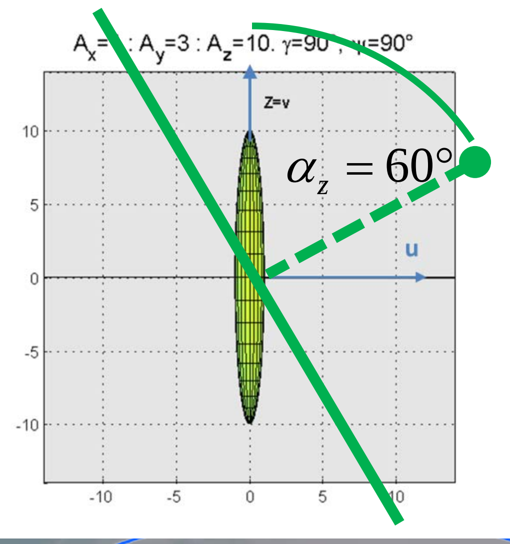

Results in Equatorial configuration

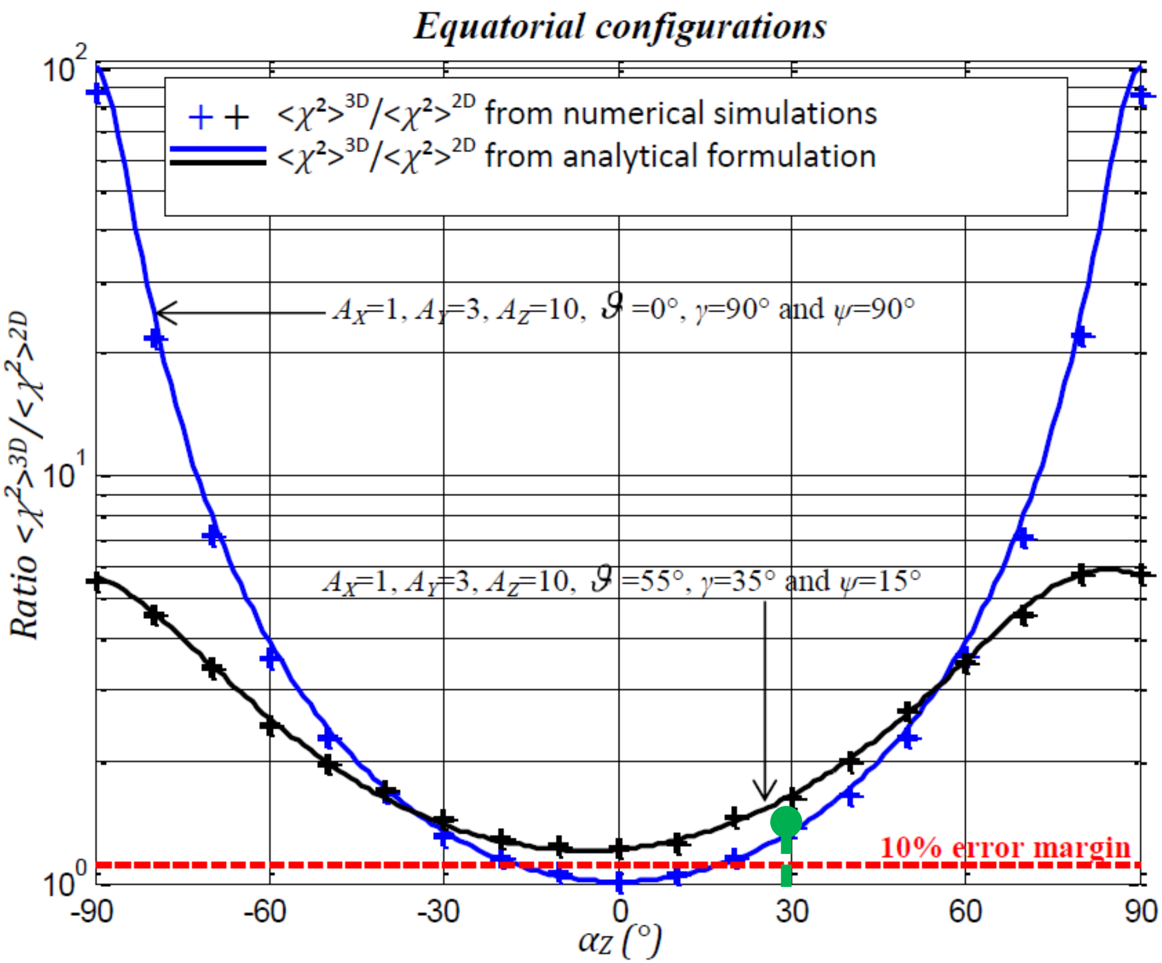

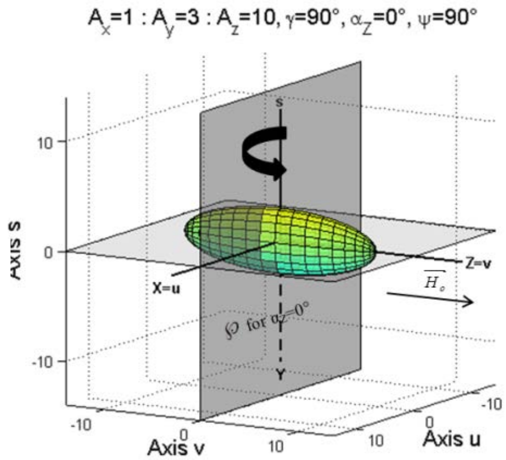

Top View (uOv)
(LOS transverse plane)

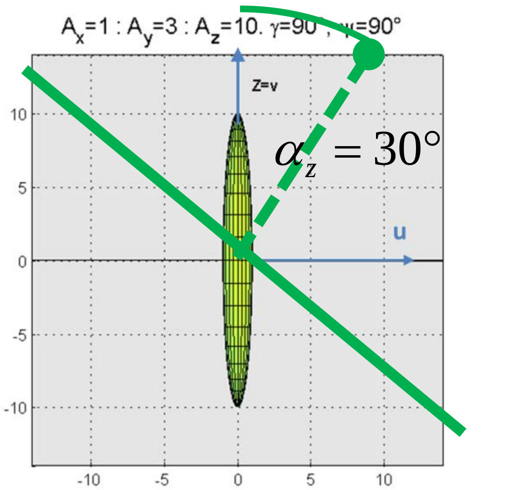

Fig.7: Ratio of log-amplitude variances derived from 3D and 2D numerical simulations (+) and analytical (-) as a function of the plane of dimensional reduction defined by α_Z

Results in Equatorial configuration

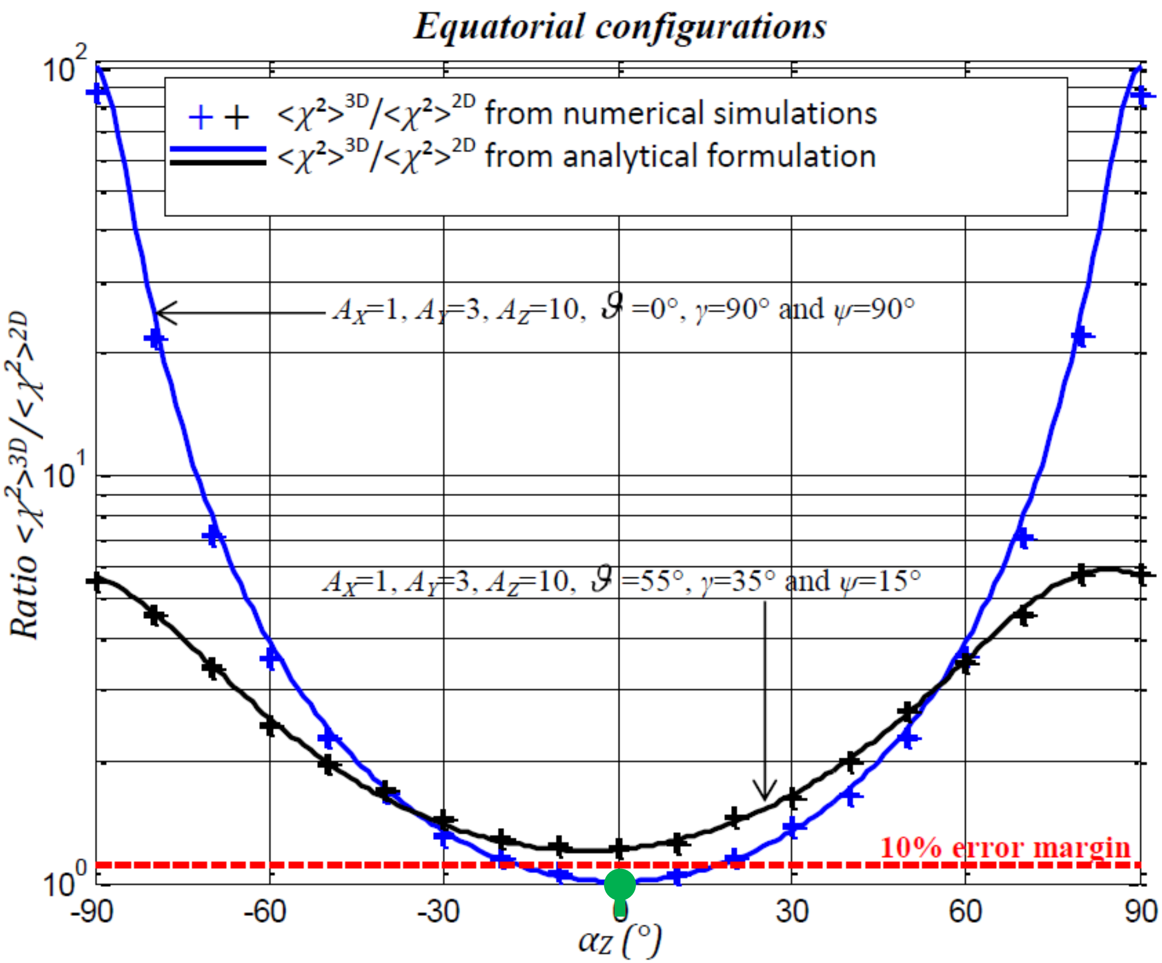

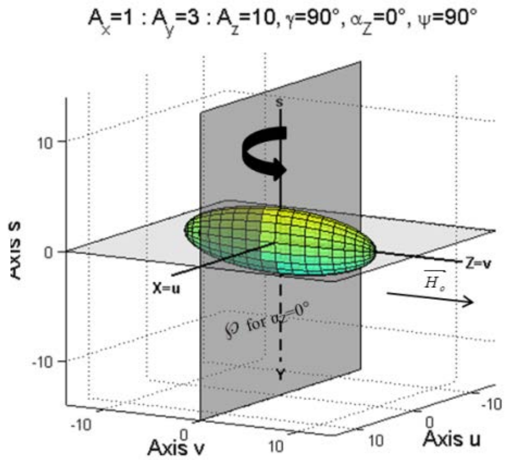

Top View (uOv)

(LOS transverse plane)

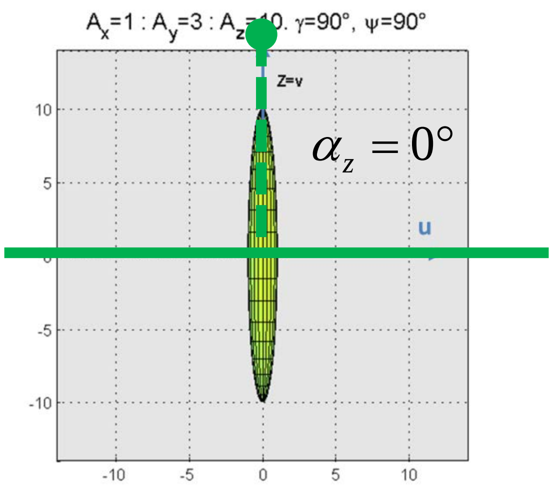

Fig.7: Ratio of log-amplitude variances derived from 3D and 2D numerical simulations (+) and analytical (-) as a function of the plane of dimensional reduction defined by α_Z

Results in Equatorial configuration

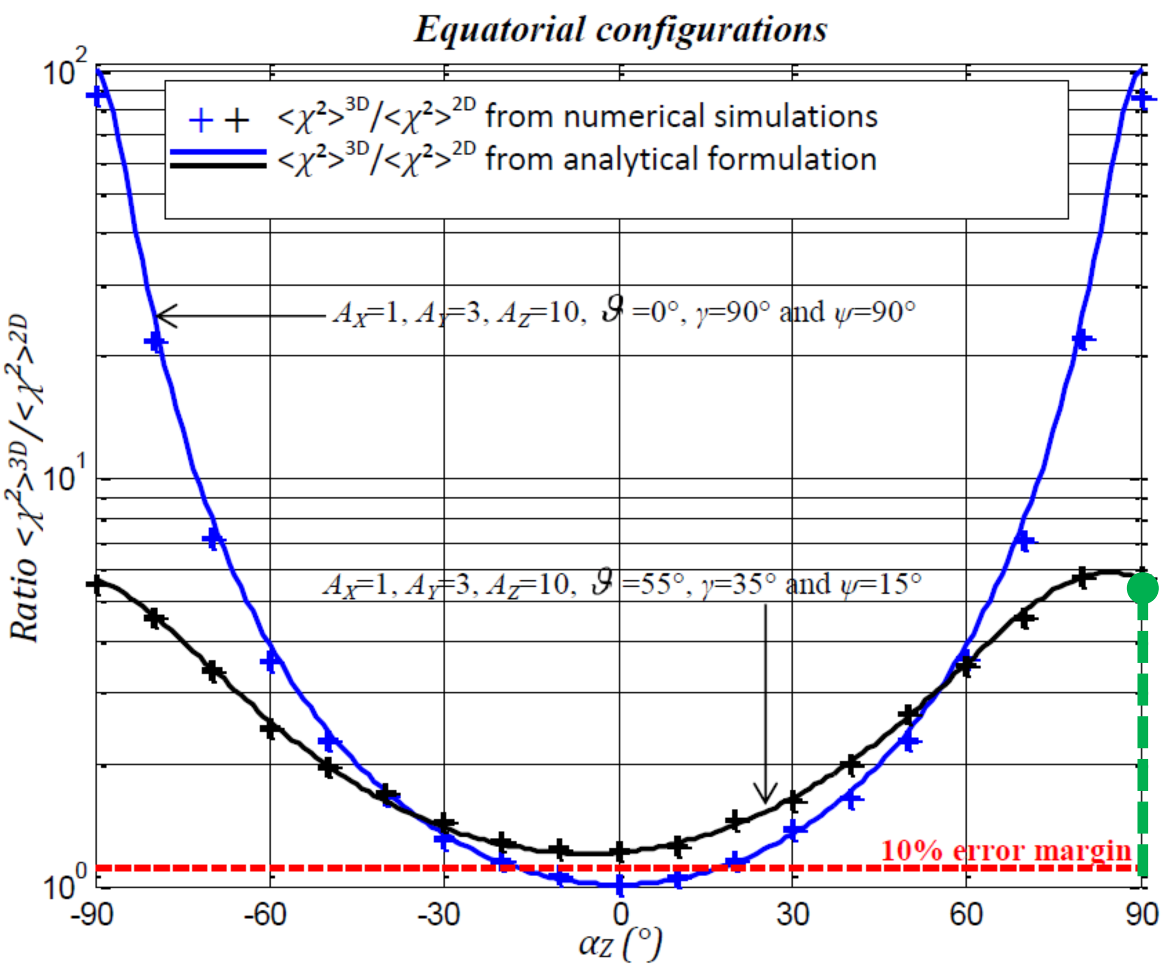

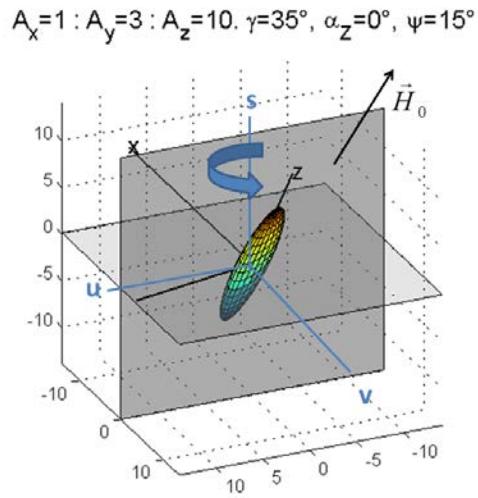

Top View (uOv)

(LOS transverse plane)

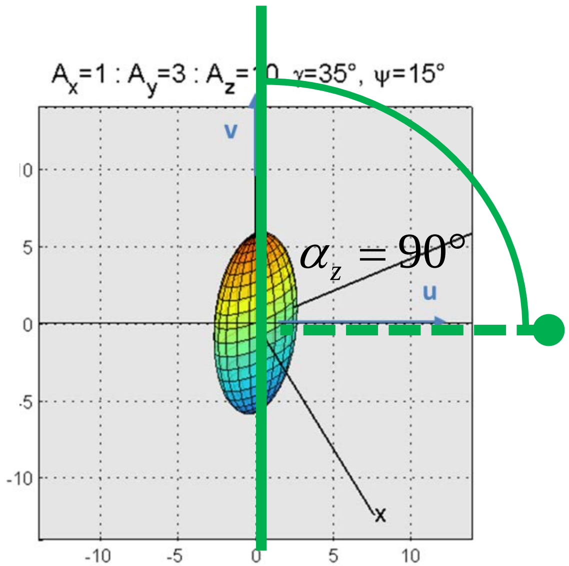

Fig.7: Ratio of log-amplitude variances derived from 3D and 2D numerical simulations (+) and analytical (-) as a function of the plane of dimensional reduction defined by α_z

Results in Equatorial configuration

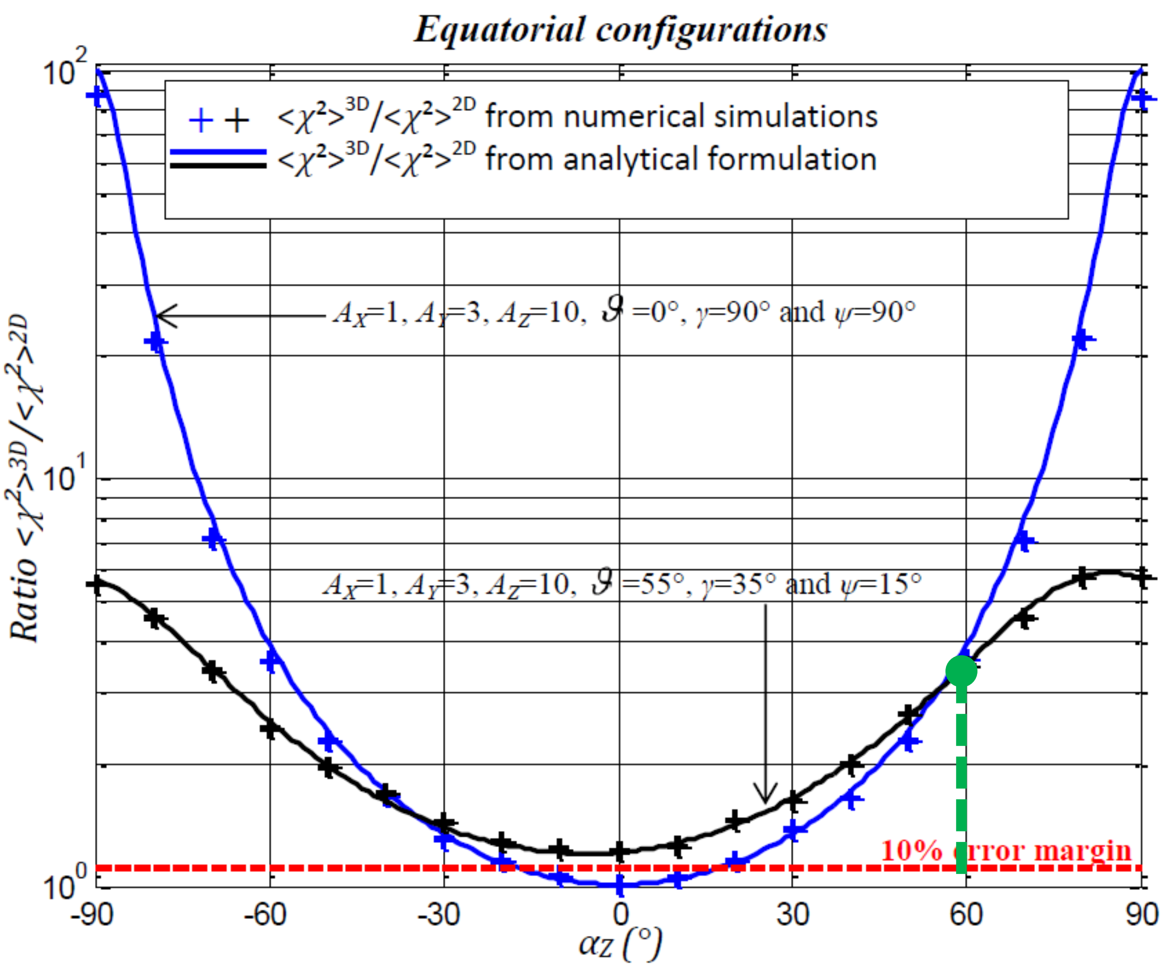

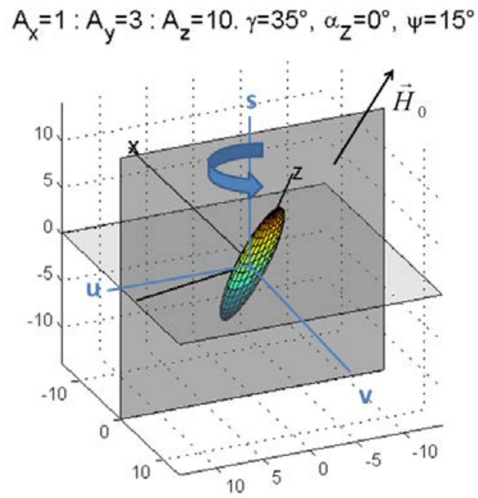

Top View (uOv)
(LOS transverse plane)

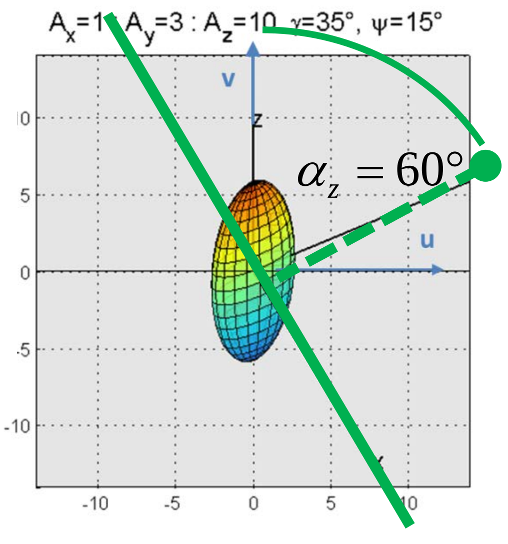

Fig.7: Ratio of log-amplitude variances derived from 3D and 2D numerical simulations (+) and analytical (-) as a function of the plane of dimensional reduction defined by α_Z

Results in Equatorial configuration

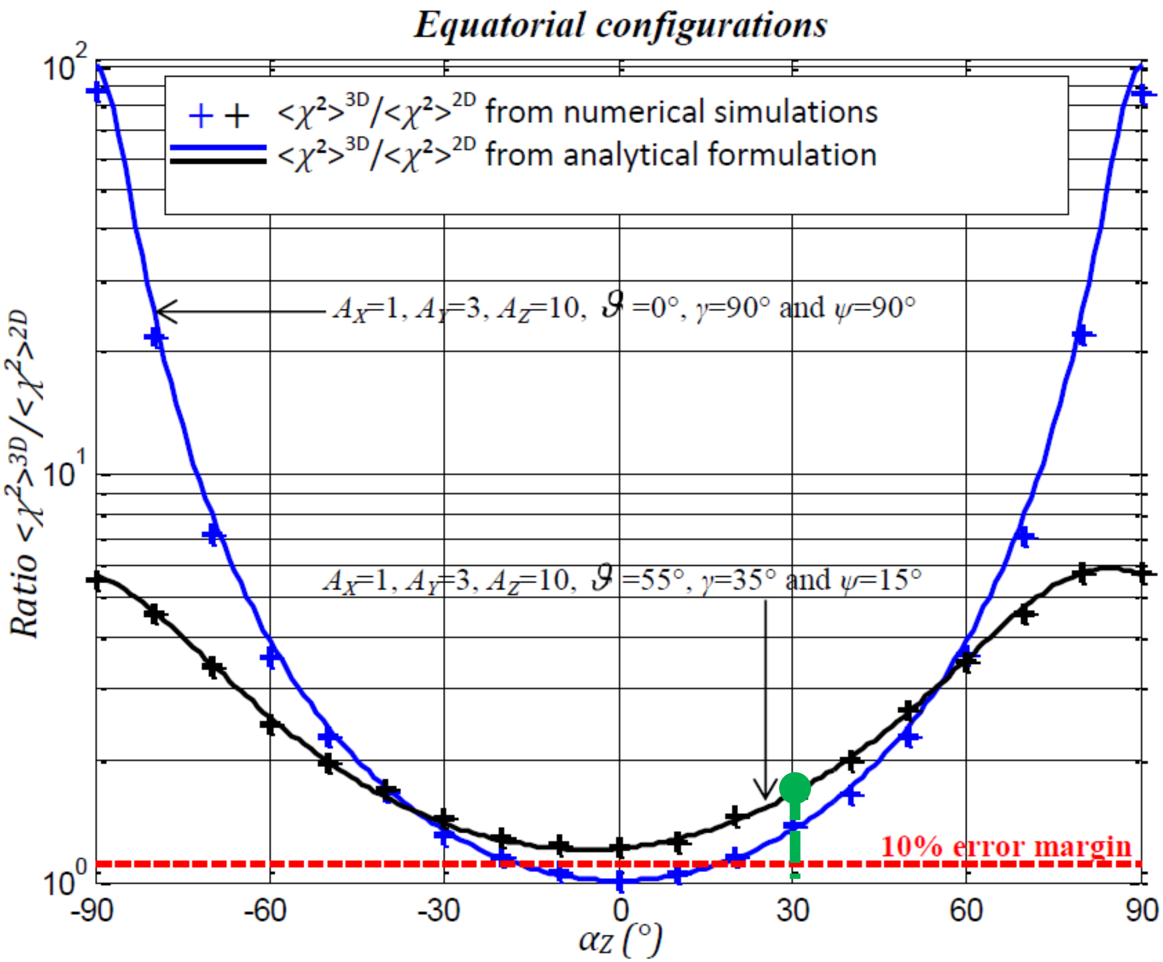

Fig.7: Ratio of log-amplitude variances derived from 3D and 2D numerical simulations (+) and analytical (-) as a function of the plane of dimensional reduction defined by α_Z

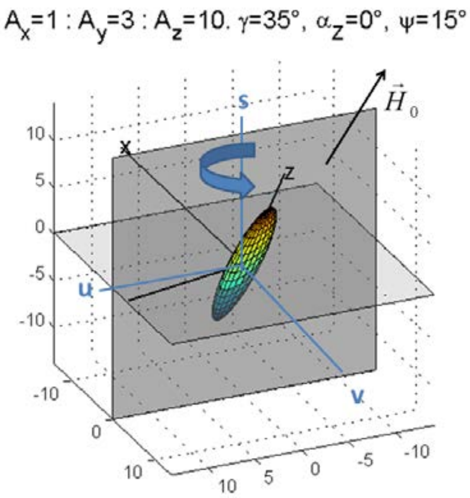

Top View (uOv)

(LOS transverse plane)

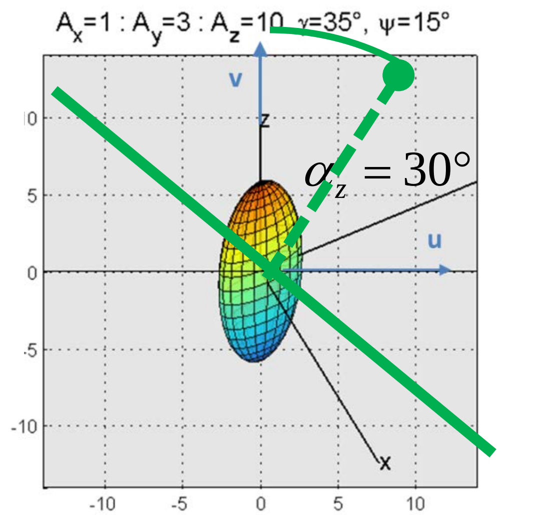

Results in Equatorial configuration

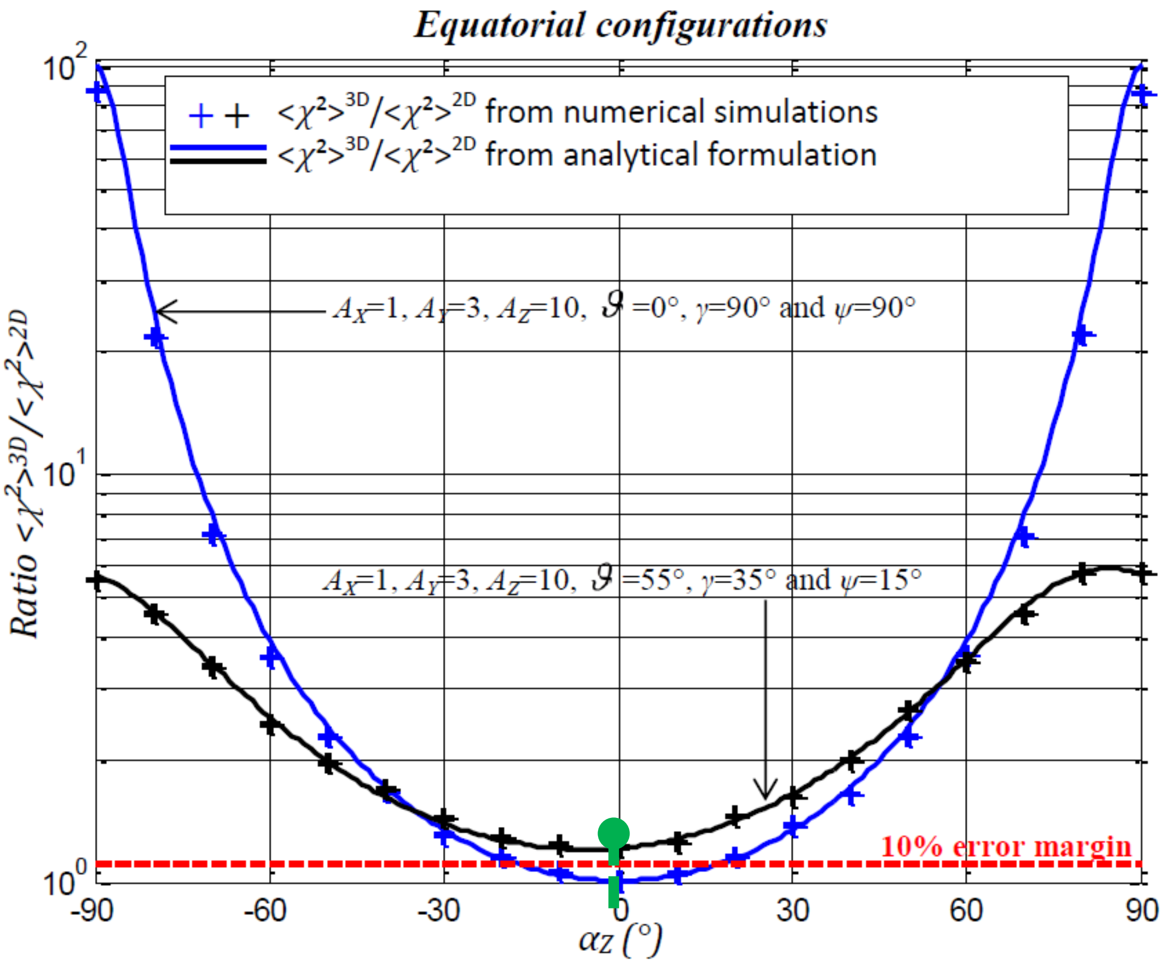

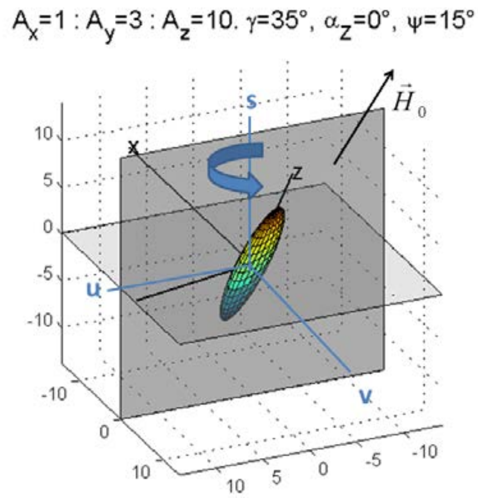

Top View (uOv)
(LOS transverse plane)

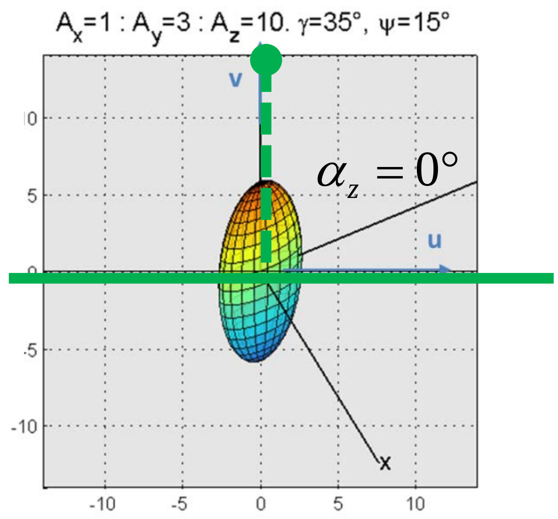

Fig.7: Ratio of log-amplitude variances derived from 3D and 2D numerical simulations (+) and analytical (-) as a function of the plane of dimensional reduction defined by α_Z

Results in Equatorial configuration

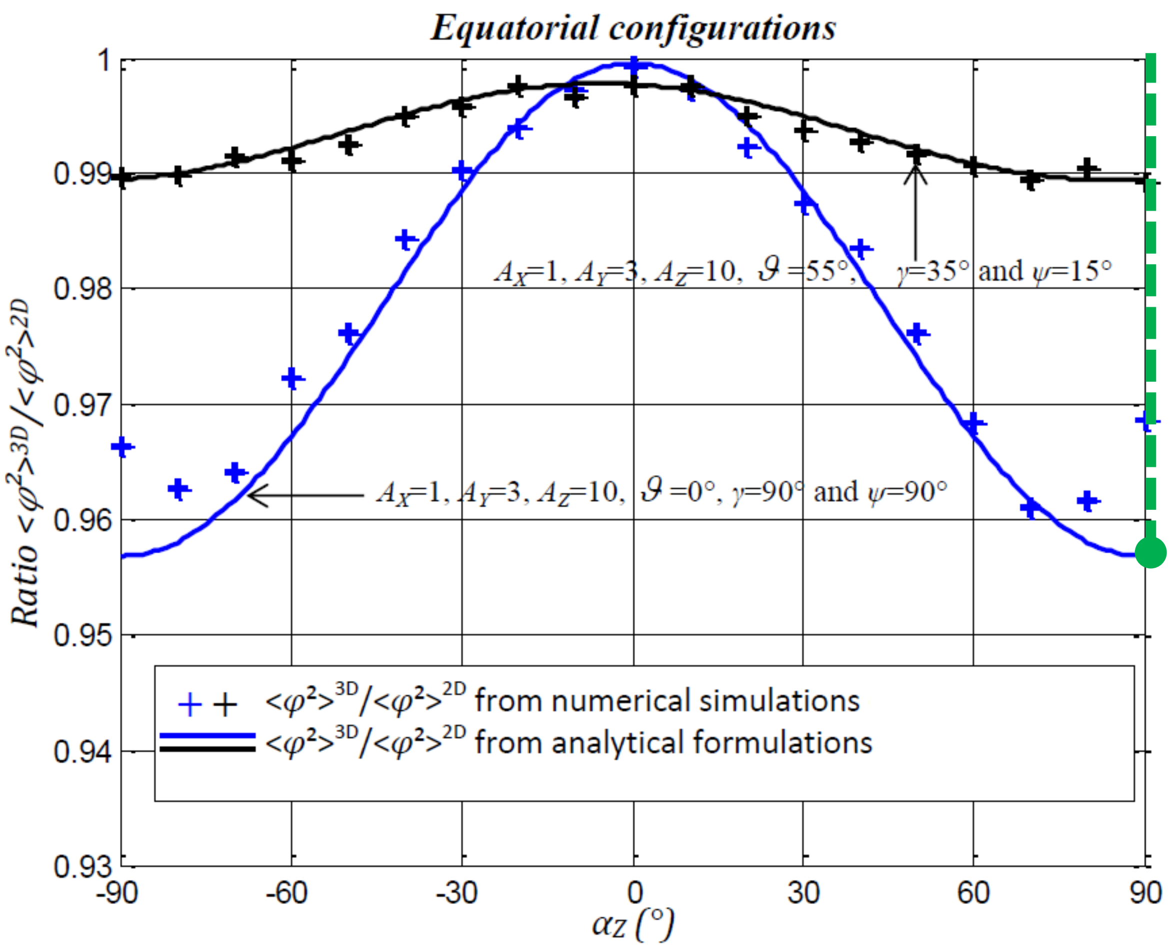

Fig.8: Ratio of phase variances derived from 3D and 2D numerical simulations (+) and analytical (-) as a function of the plane of dimensional reduction defined by α_Z

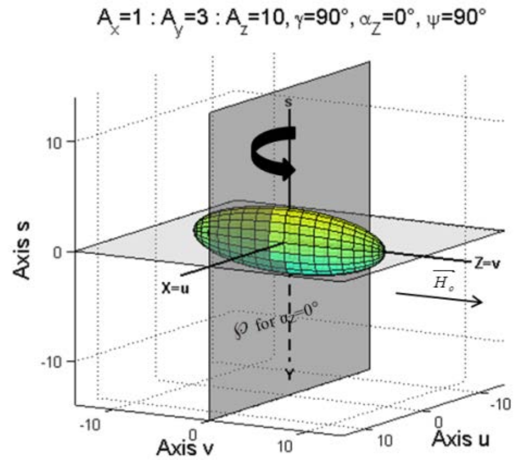

Top View (uOv)
(LOS transverse plane)

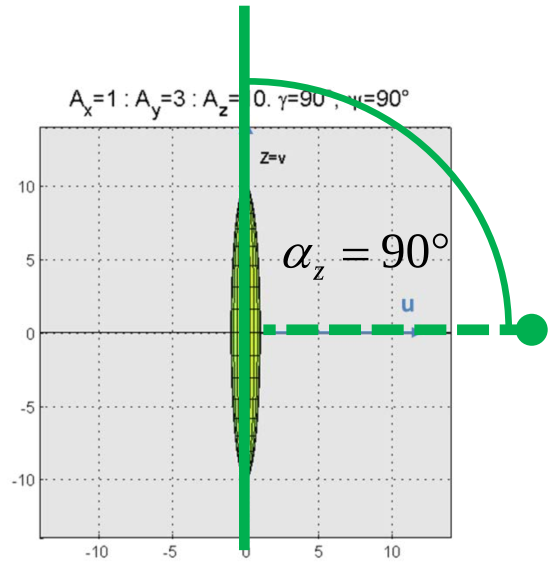

Results in Equatorial configuration

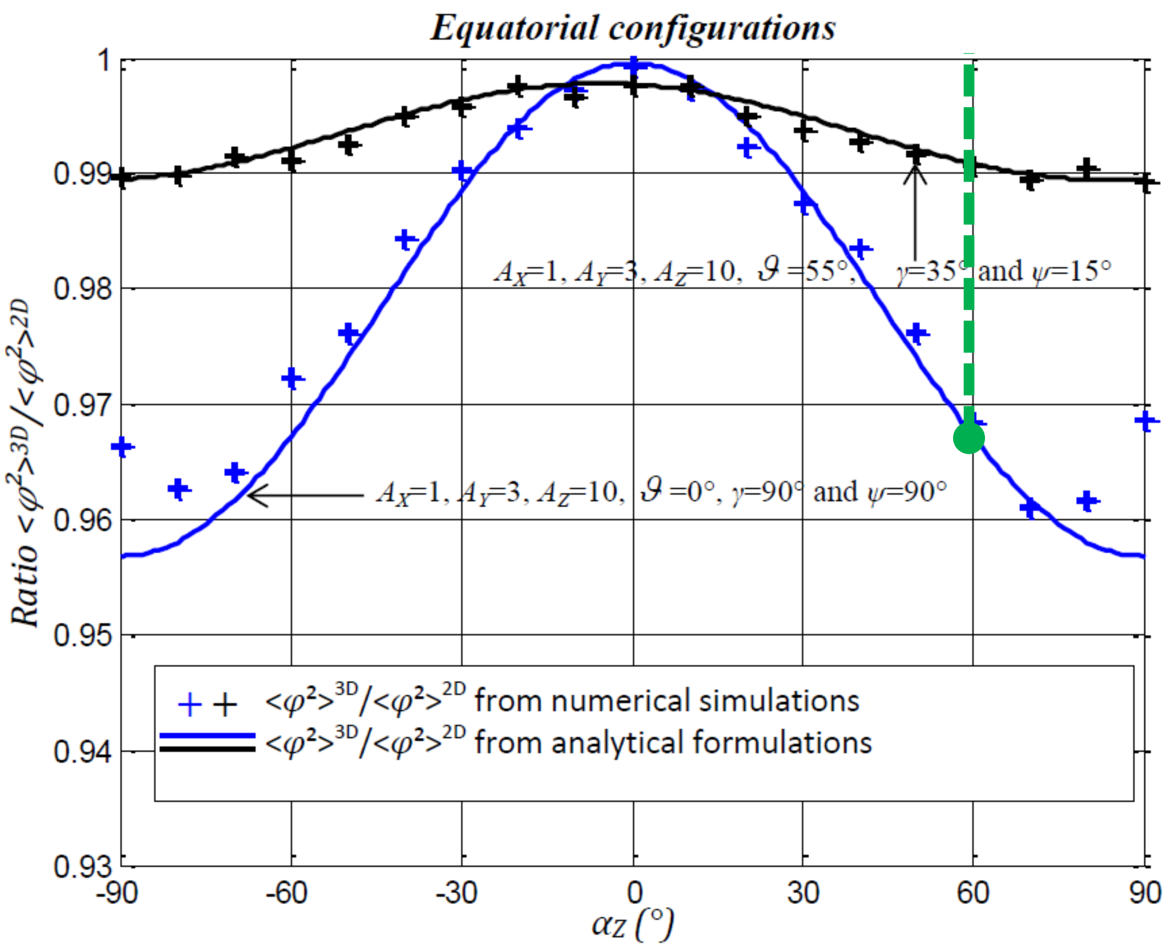

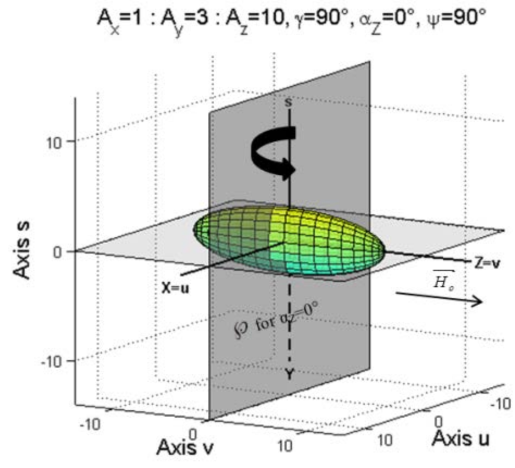

Top View (uOv)
(LOS transverse plane)

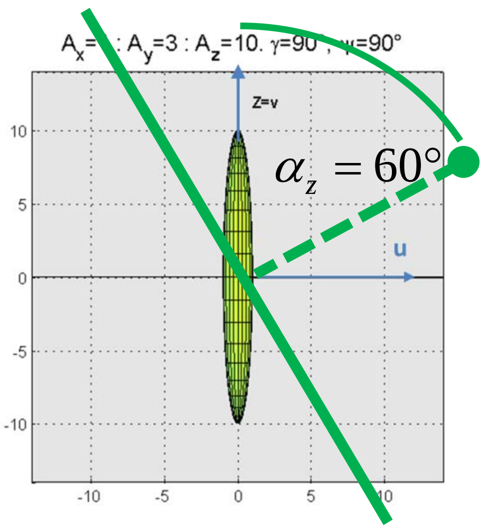

Fig.8: Ratio of phase variances derived from 3D and 2D numerical simulations (+) and analytical (-) as a function of the plane of dimensional reduction defined by α_Z

Results in Equatorial configuration

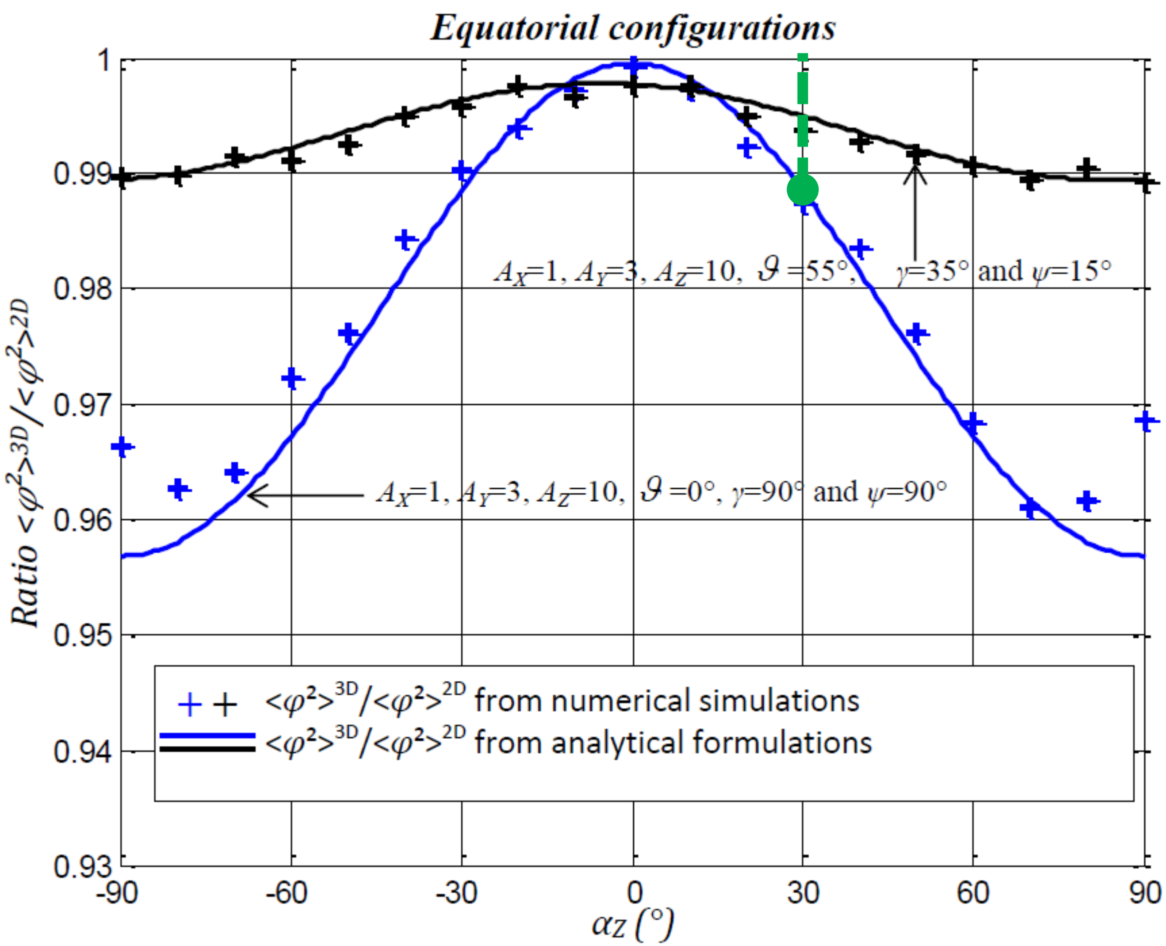

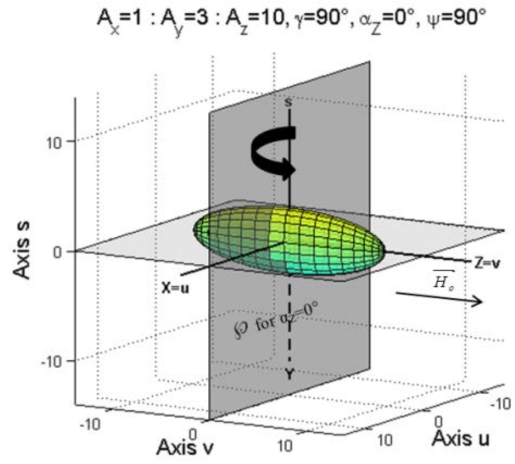

Top View (uOv)
(LOS transverse plane)

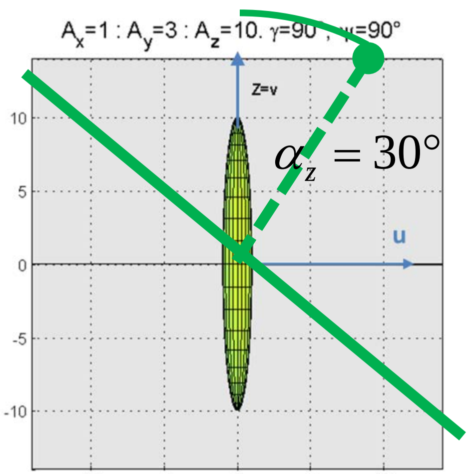

Fig.8: Ratio of phase variances derived from 3D and 2D numerical simulations (+) and analytical (-) as a function of the plane of dimensional reduction defined by α_Z

Results in Equatorial configuration

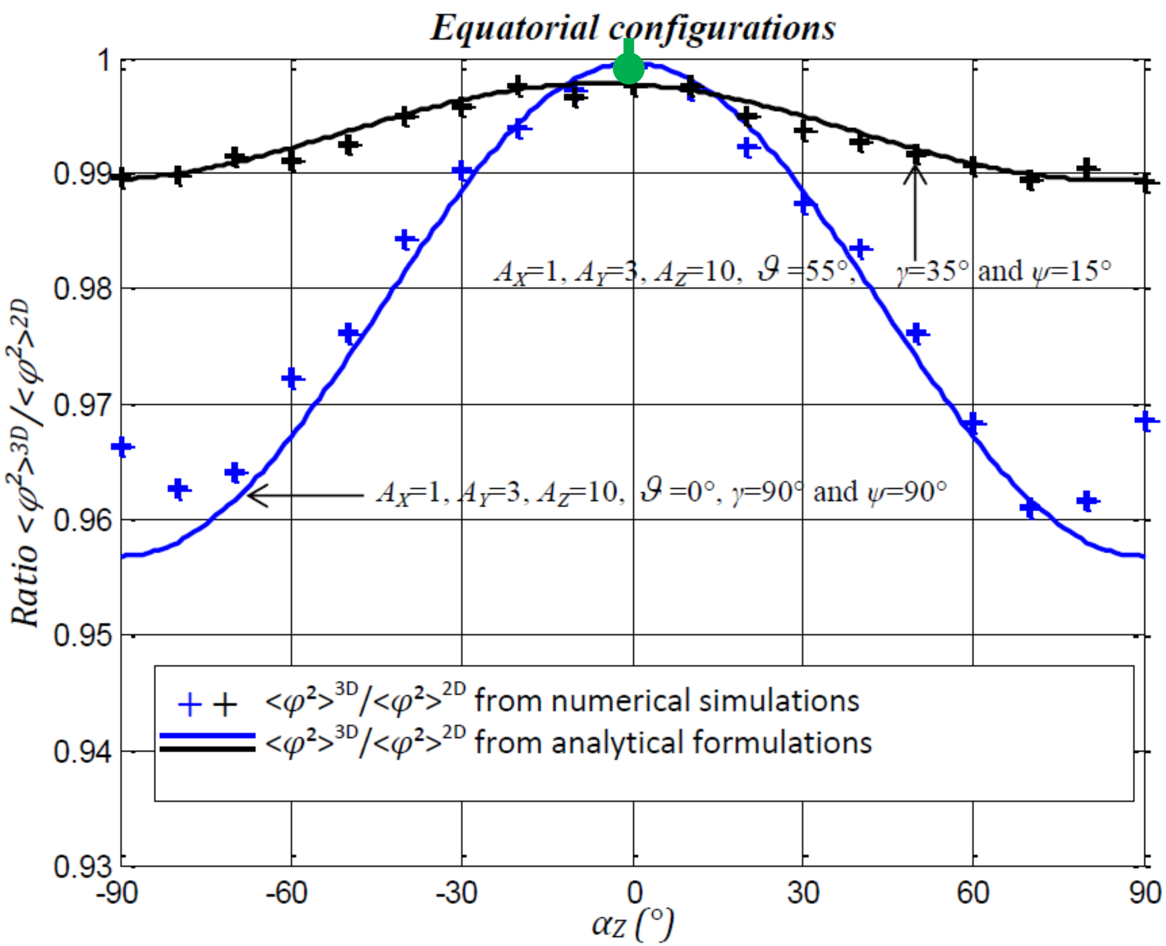

Fig.8: Ratio of phase variances derived from 3D and 2D numerical simulations (+) and analytical (-) as a function of the plane of dimensional reduction defined by α_Z

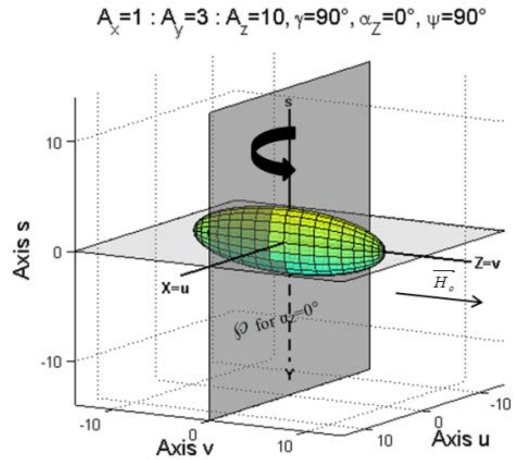

Top View (uOv)
(LOS transverse plane)

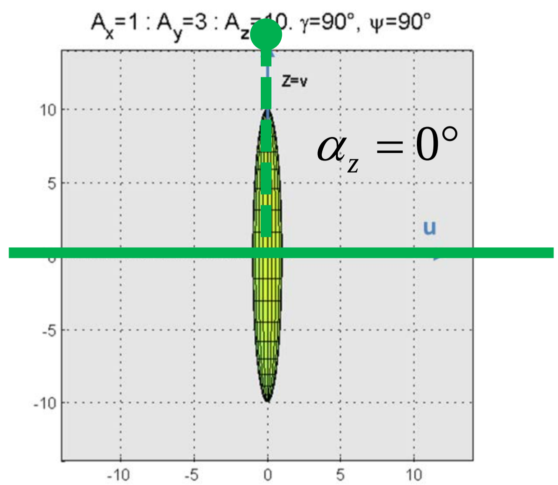

Results in Equatorial configuration

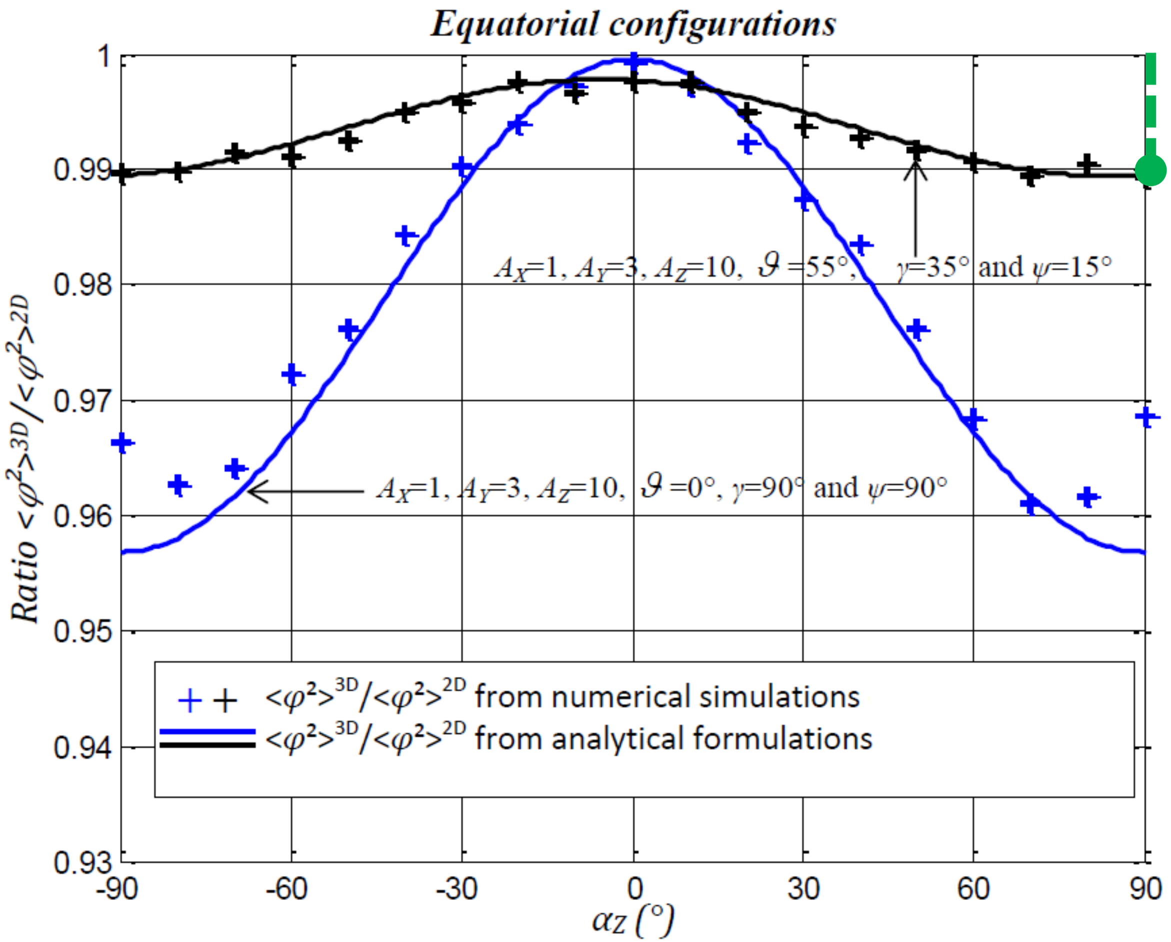

Fig.8: Ratio of phase variances derived from 3D and 2D numerical simulations (+) and analytical (-) as a function of the plane of dimensional reduction defined by α_Z

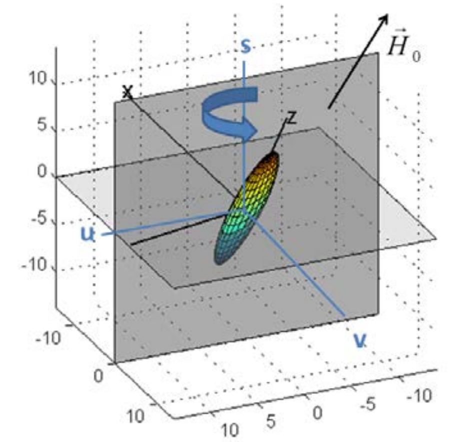

Top View (uOv)
(LOS transverse plane)

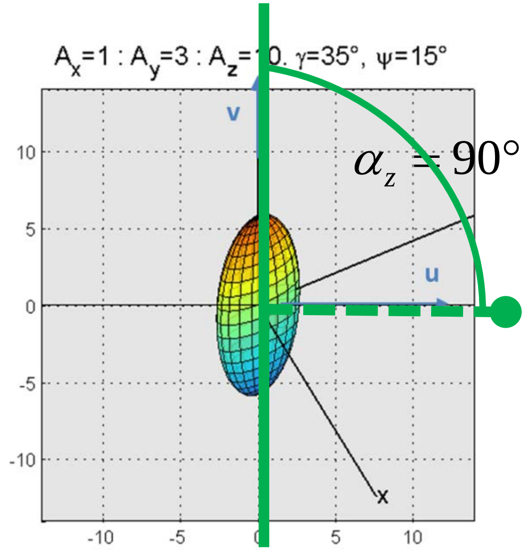

Results in Equatorial configuration

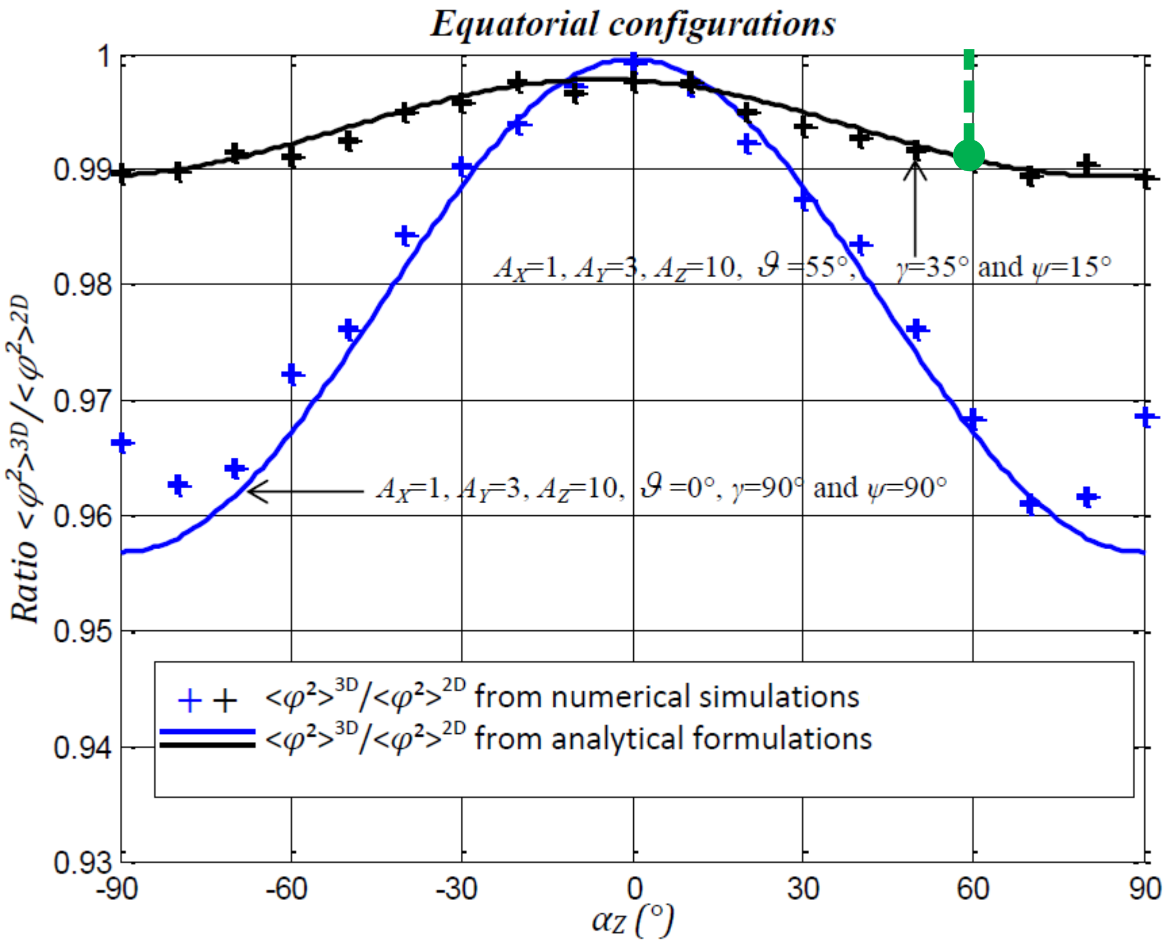

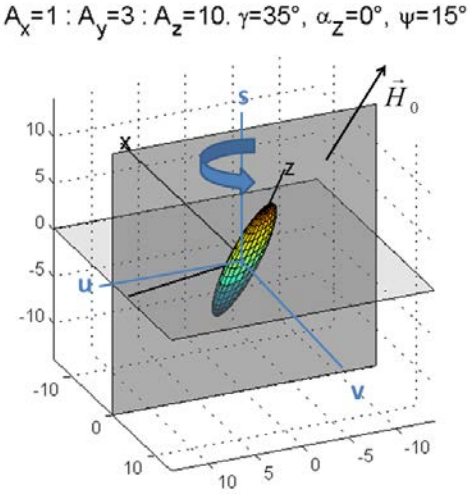

Top View (uOv)
(LOS transverse plane)

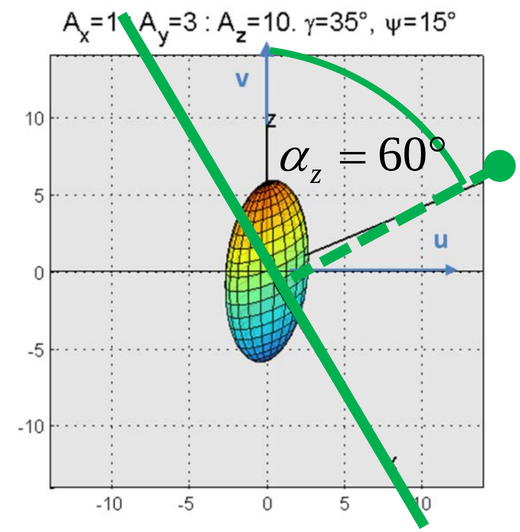

Fig.8: Ratio of phase variances derived from 3D and 2D numerical simulations (+) and analytical (-) as a function of the plane of dimensional reduction defined by α_Z

Results in Equatorial configuration

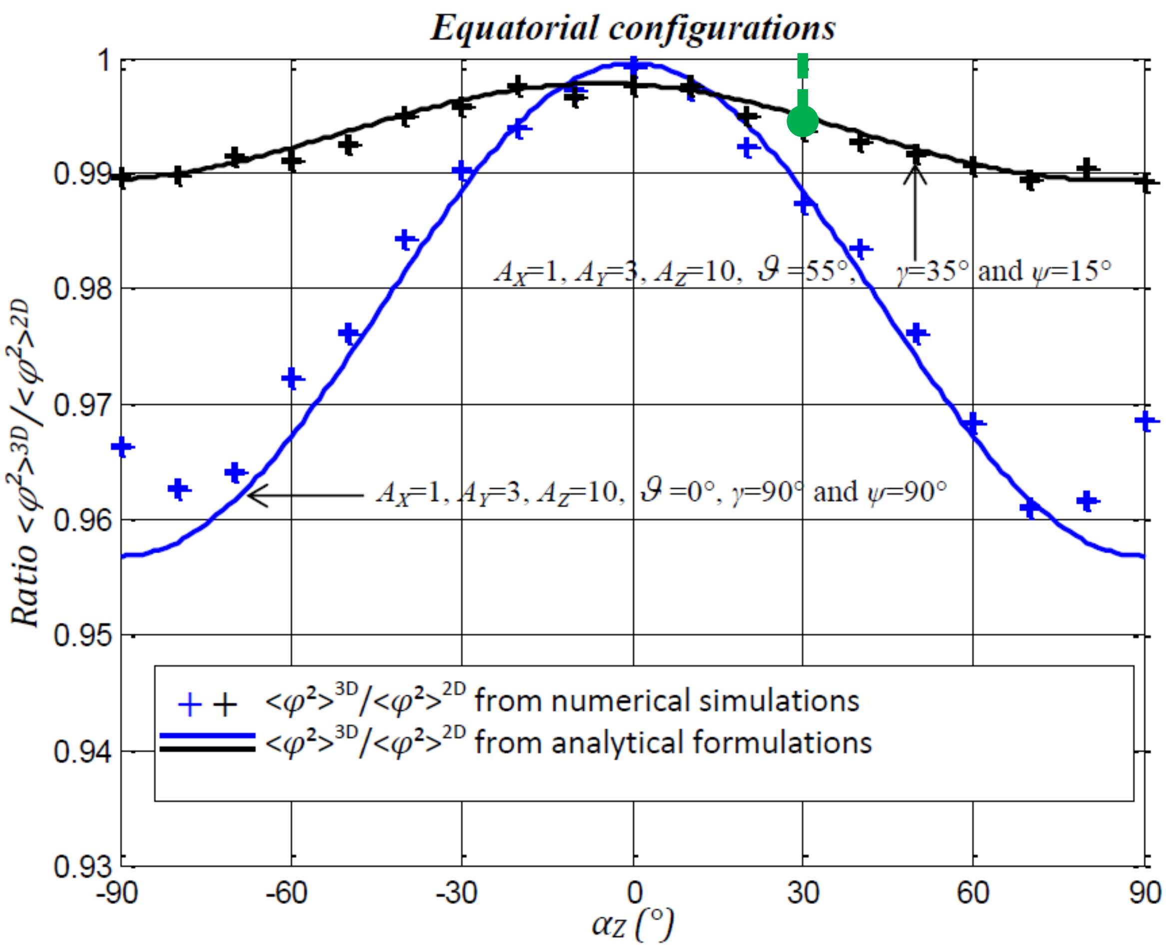

Fig.8: Ratio of phase variances derived from 3D and 2D numerical simulations (+) and analytical (-) as a function of the plane of dimensional reduction defined by α_Z

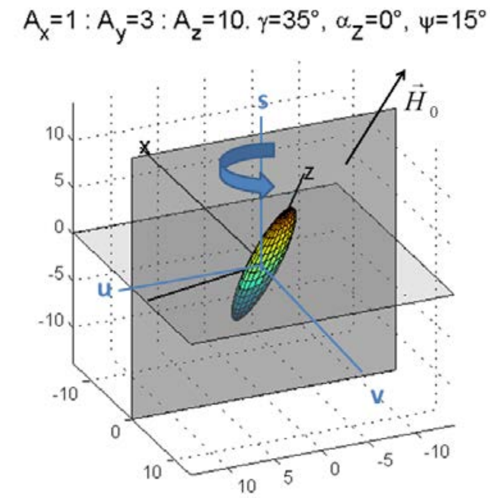

Top View (uOv)
(LOS transverse plane)

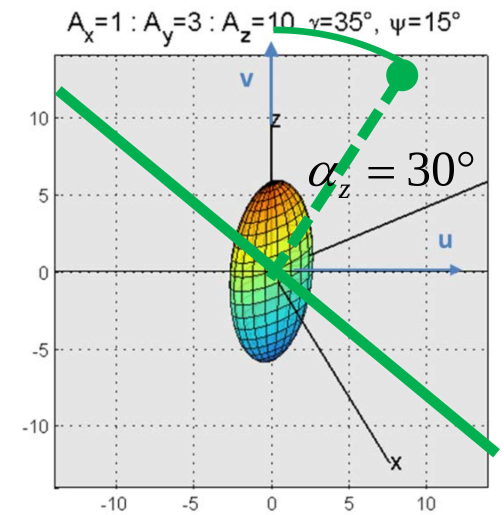

Results in Equatorial configuration

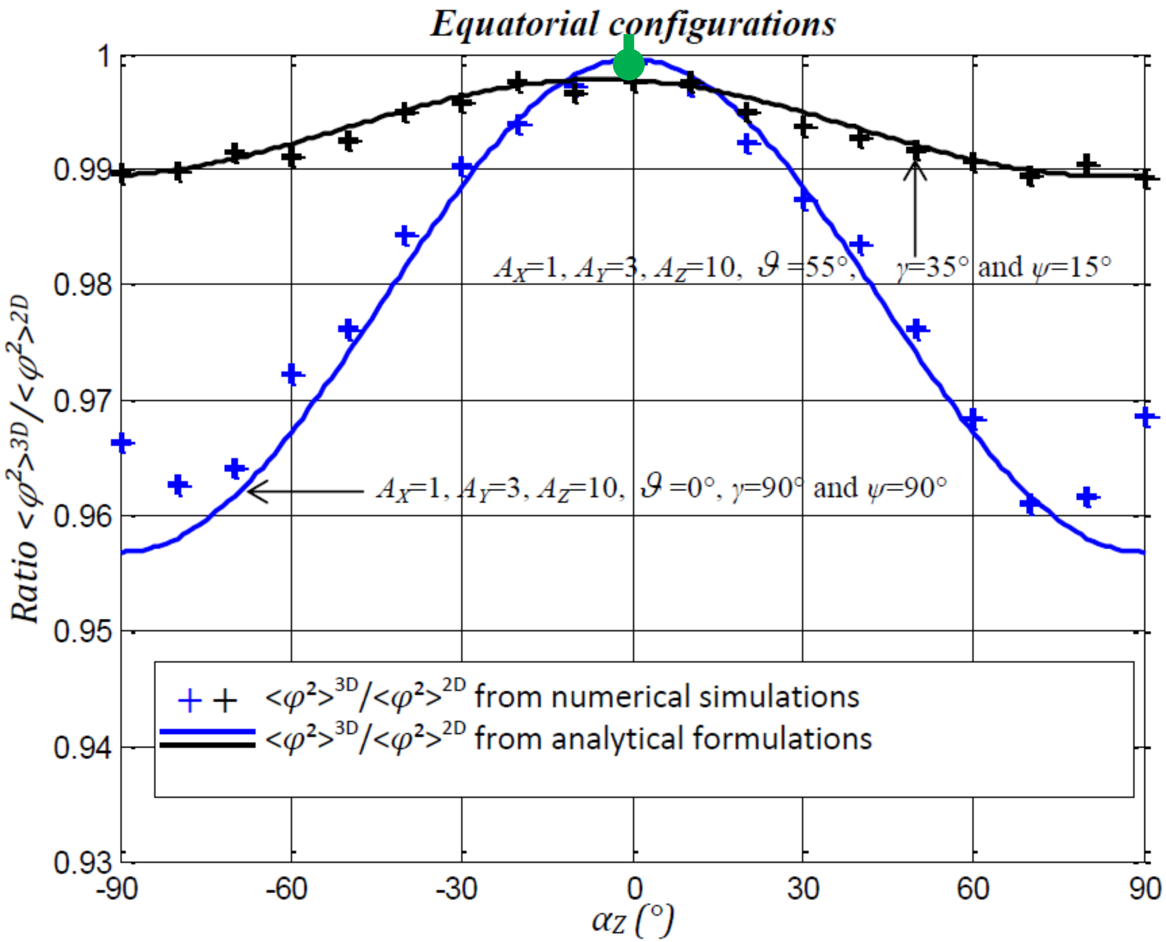

Fig.8: Ratio of phase variances derived from 3D and 2D numerical simulations (+) and analytical (-) as a function of the plane of dimensional reduction defined by α_Z

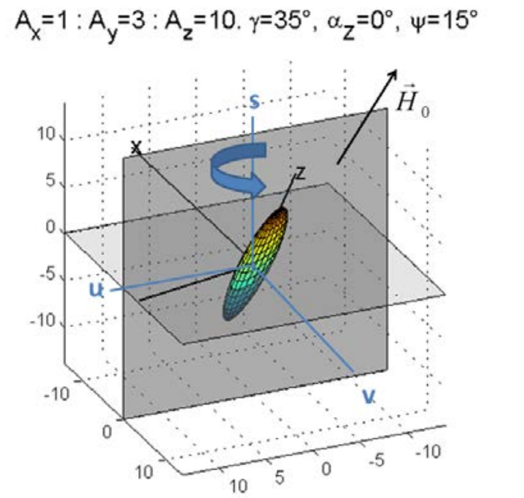

Top View (uOv)
(LOS transverse plane)

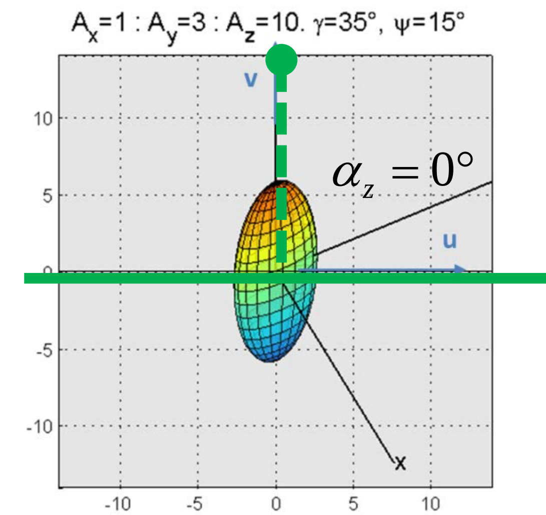

Results in Equatorial configuration

Whatever the configuration:

- **2D**-PWE/1D-MPS numerical schemes **underestimates** 3D log-amplitude variances in proportions that depends on the plane of dimentional reduction (from 1 up to 87,2)
- **2D** numerical schemes slightly **overestimate** 3D phase variances (from 0,96 up to 1)

If one accepts an error of 10%:

- For equatorial case, then 2D numerical schemes can be safely used **for α_z less than ~20°**
- For second equatorial configuration, the optimal plane of dimensional reduction around **α_z = 0, introduces an error of 22%,** i.e. well beyond the error margin arbitrarily fixed to 10 %

3D to 2D approximation effect on propagation modeling, impact on scintillation indices

Content

- Propagation geometry and medium description
- 3D and 2D numerical schemes
- 3D and 2D analytical derivations
- Results in equatorial configuration
- **Results in polar configuration**
- Conclusions

Results in Polar configuration

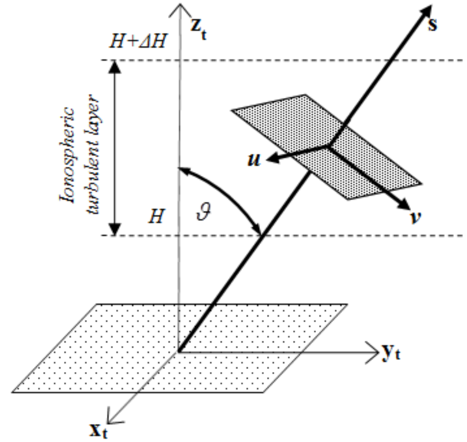

2 polar configurations considered:

[*Livingston et al.*, 1982], [*Gola*, 1992]

sheet-like ionospheric irregularities

field-aligned rods

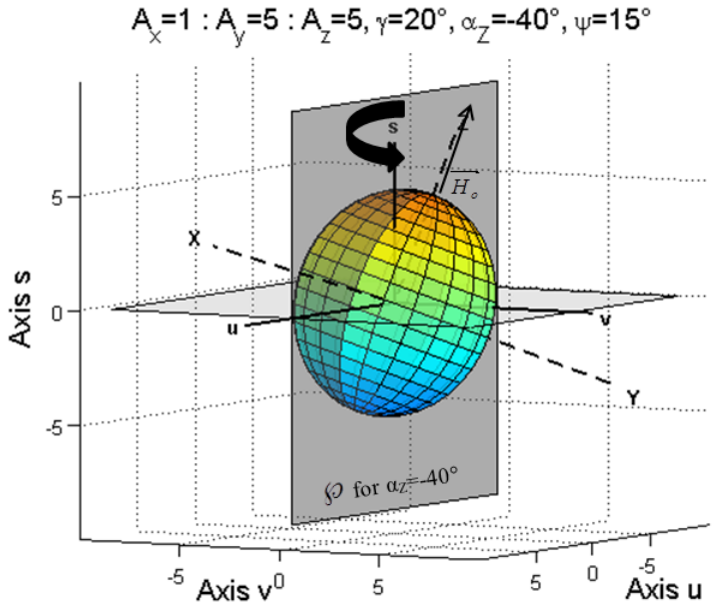

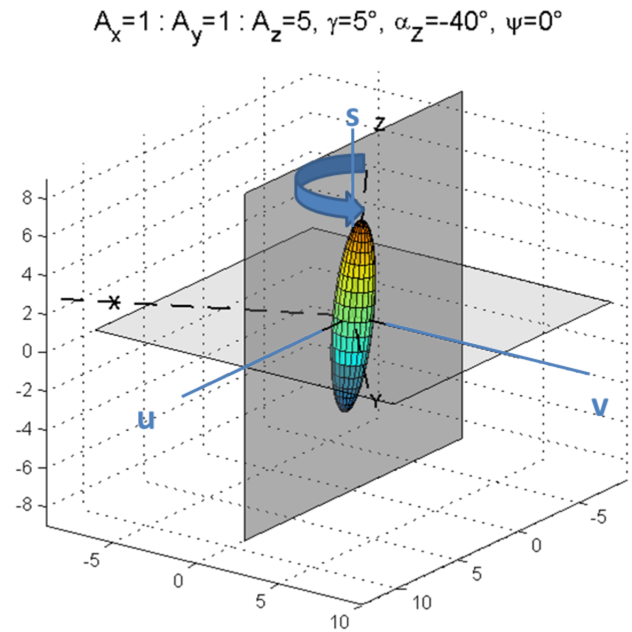

Fig.9: Ionospheric irregularity in the LOS coordinate system *(u,v,s)* for the 1st polar configuration

Fig.10: Ionospheric irregularity in the LOS coordinate system *(u,v,s)* for the 2nd polar configuration

Results in Polar configuration

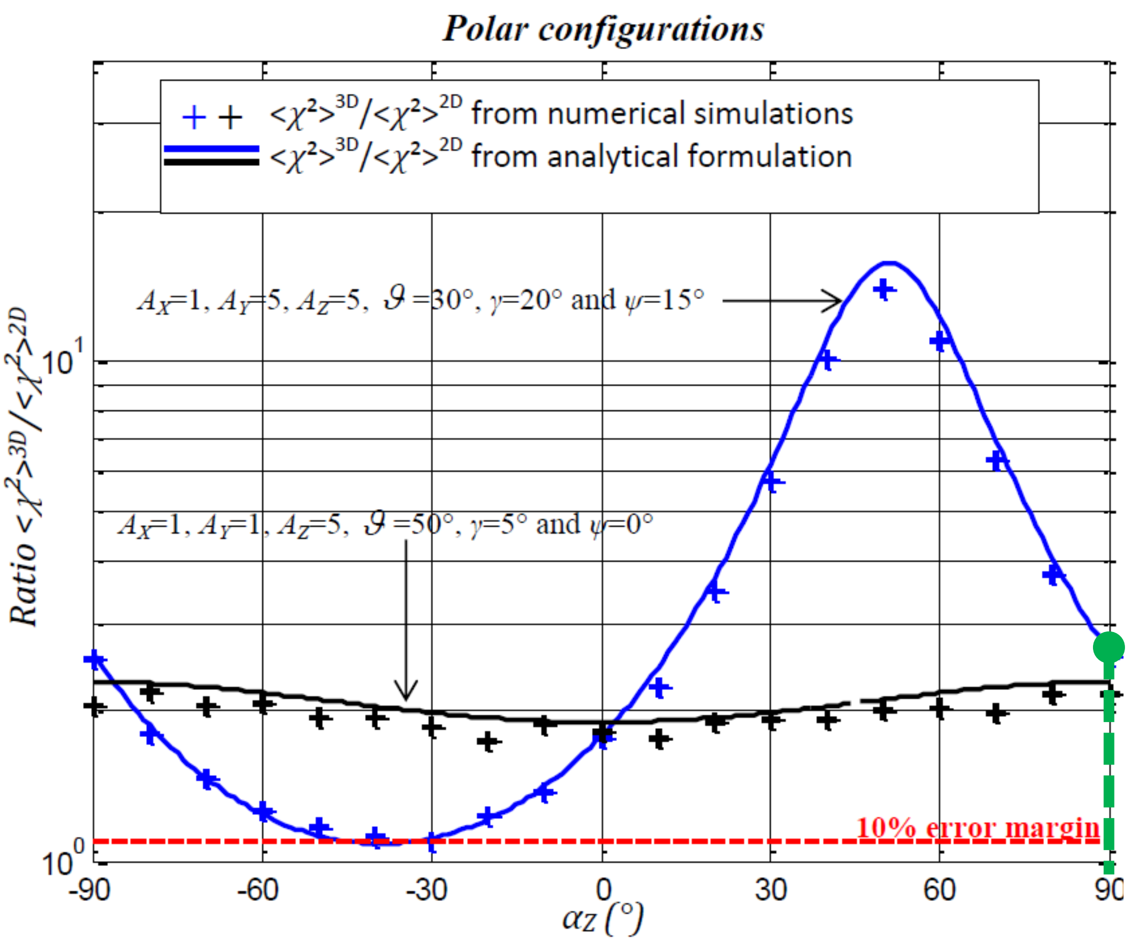

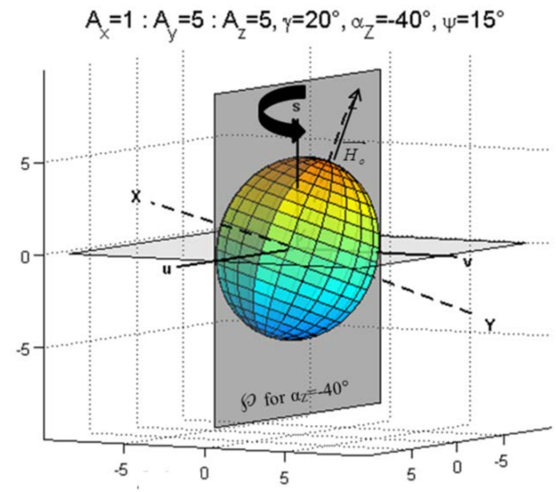

Top View (uOv)
(LOS transverse plane)

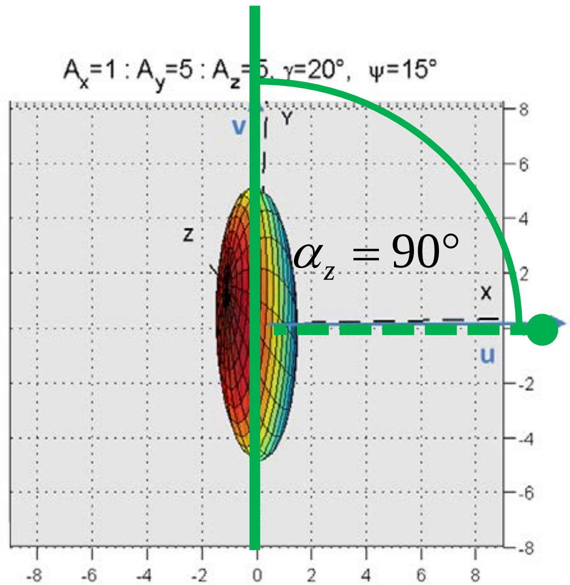

Fig.11: Ratio of log-amplitude variances derived from 3D and 2D numerical simulations (+) and analytical (-) as a function of the plane of dimensional reduction defined by α_Z

Results in Polar configuration

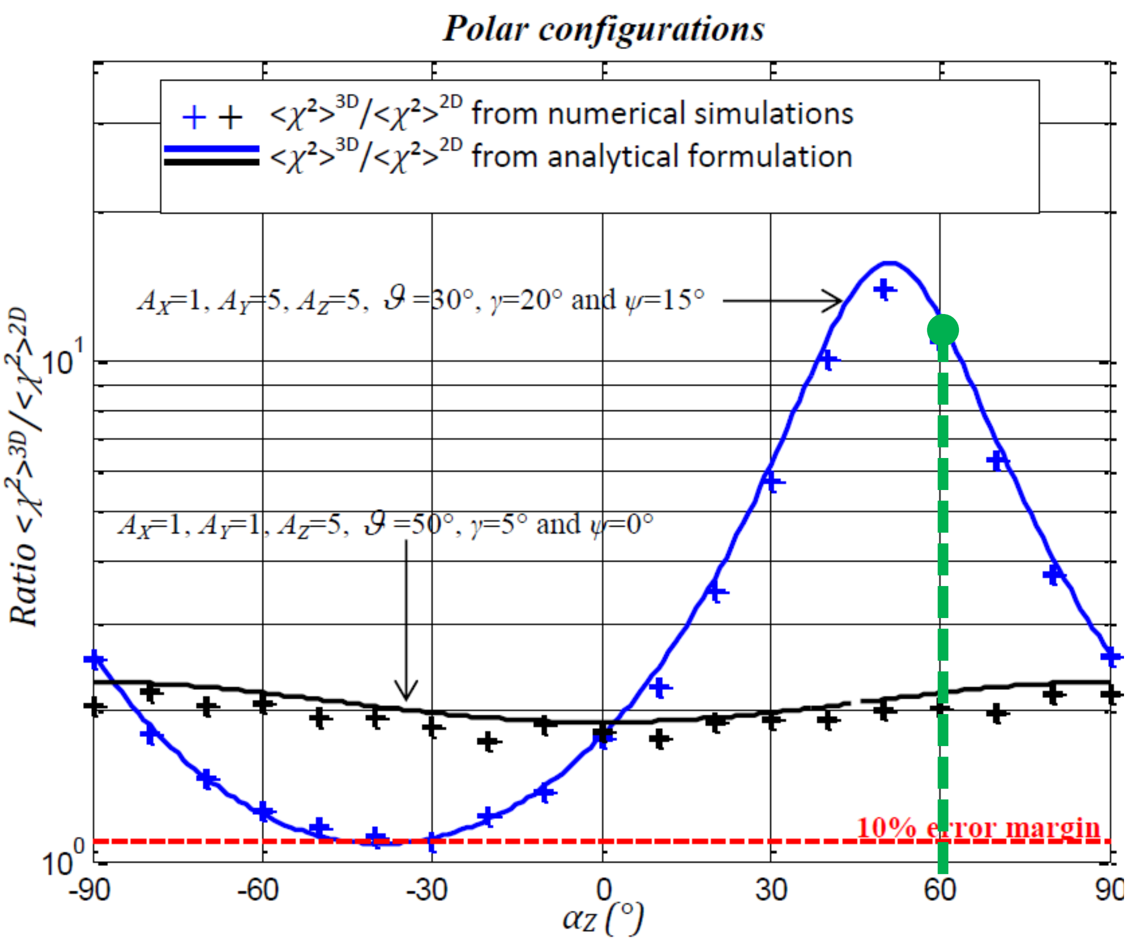

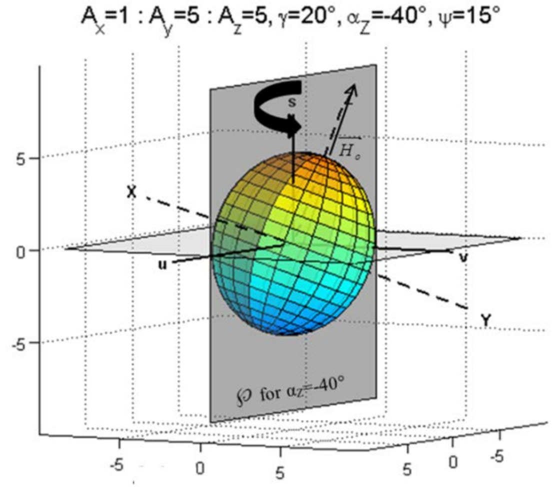

Top View (uOv)
(LOS transverse plane)

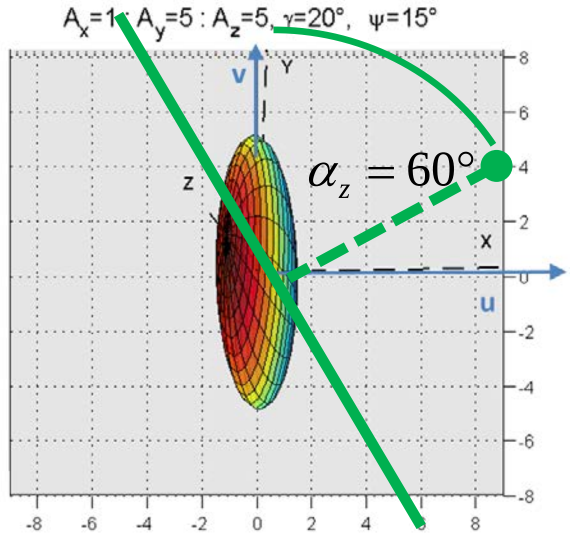

Fig.11: Ratio of log-amplitude variances derived from 3D and 2D numerical simulations (+) and analytical (-) as a function of the plane of dimensional reduction defined by α_Z

Results in Polar configuration

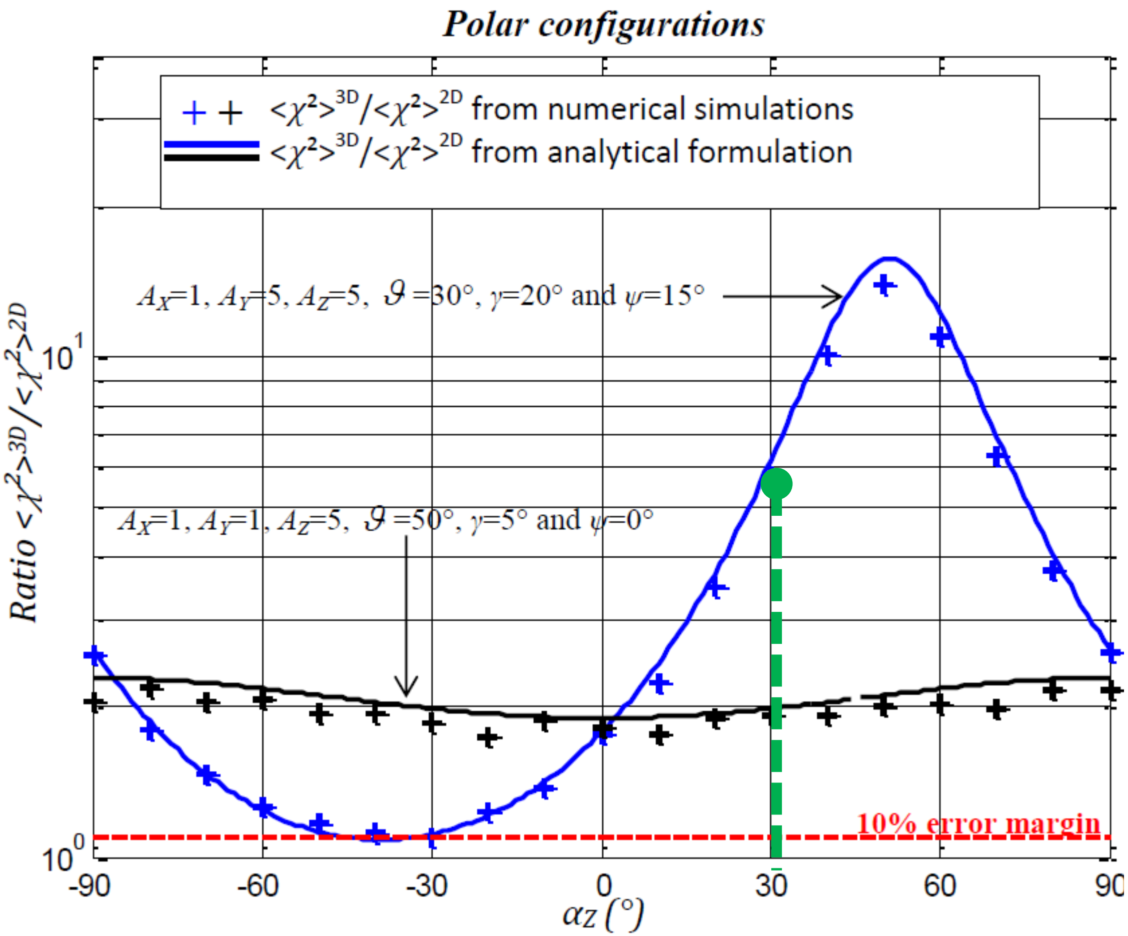

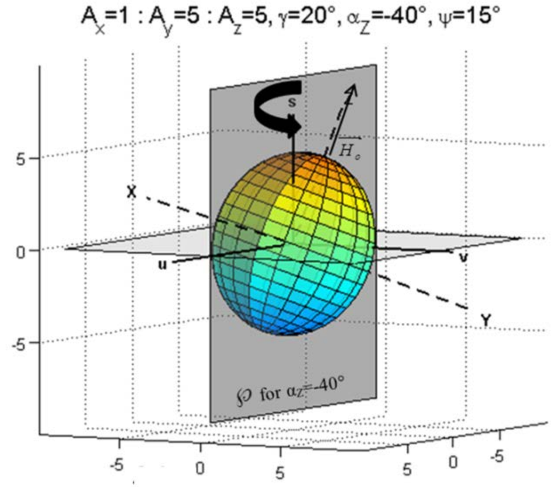

Top View (uOv)

(LOS transverse plane)

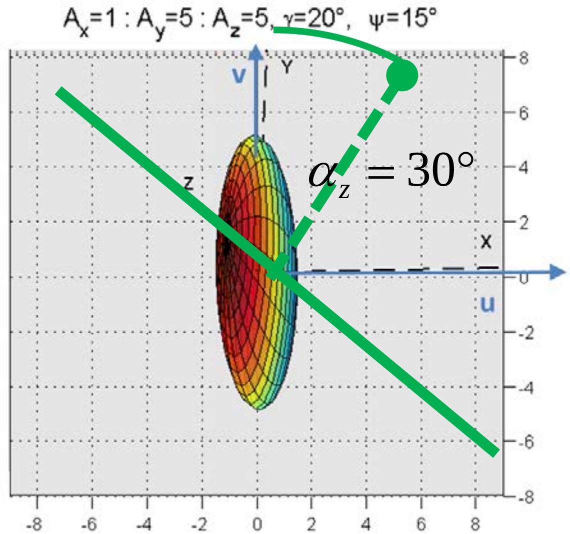

Fig.11: Ratio of log-amplitude variances derived from 3D and 2D numerical simulations (+) and analytical (-) as a function of the plane of dimensional reduction defined by α_Z

Results in Polar configuration

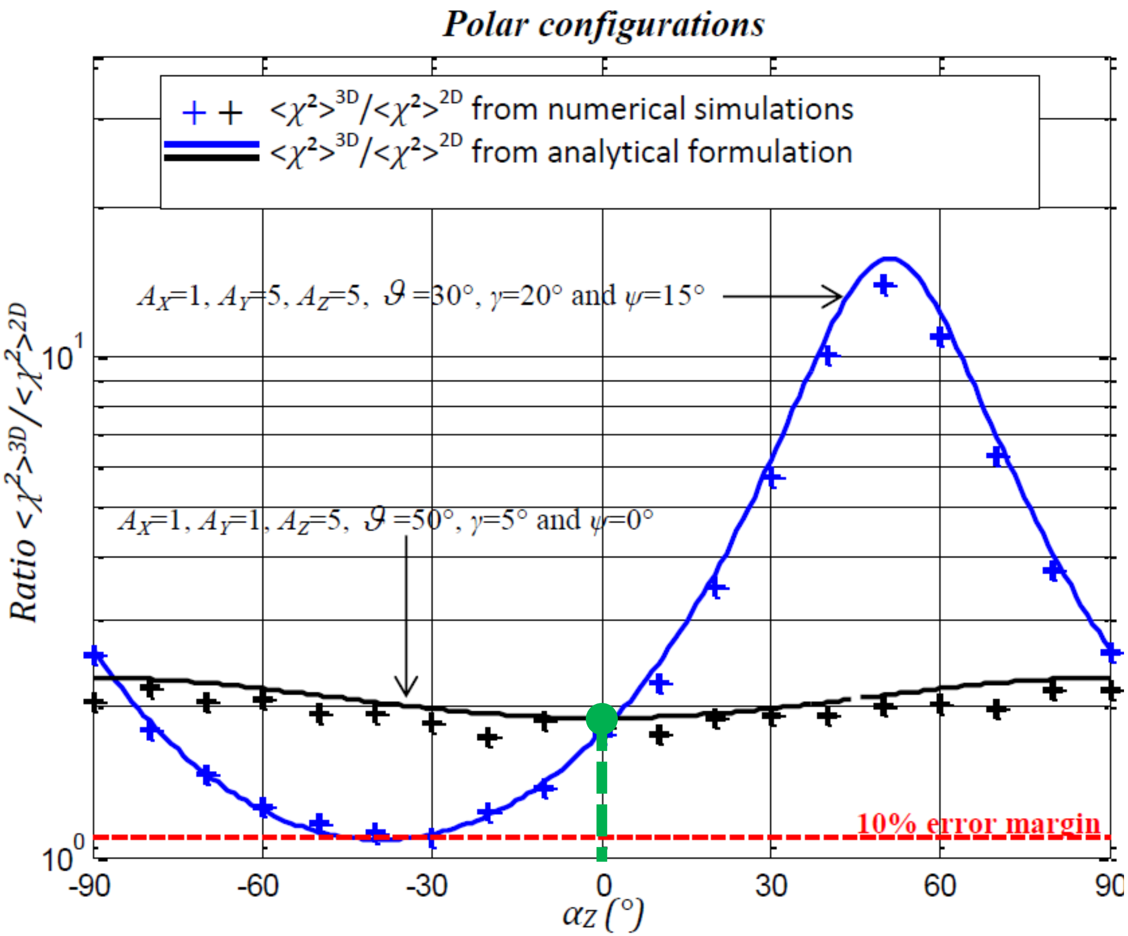

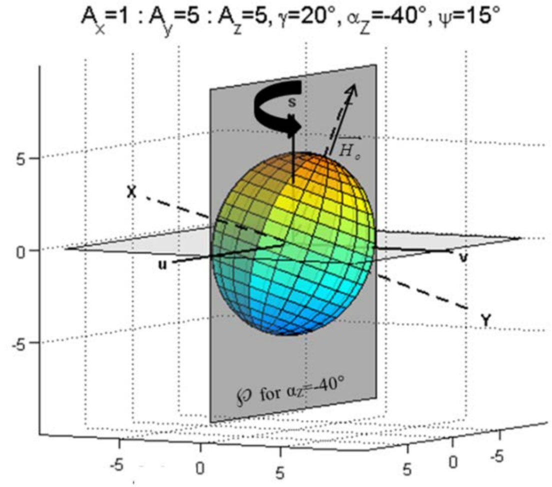

Top View (uOv)
(LOS transverse plane)

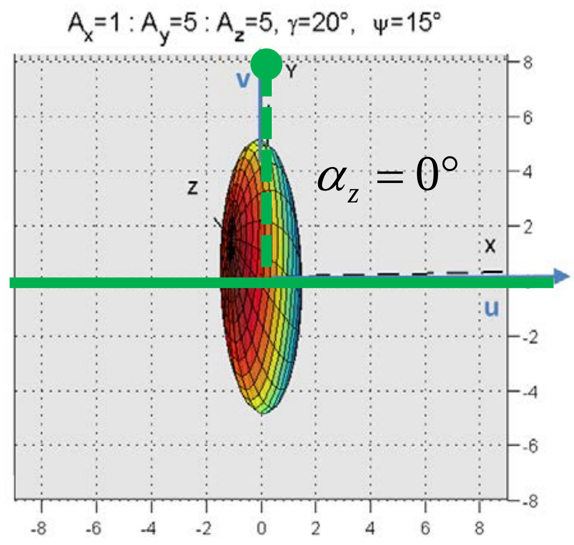

Fig.11: Ratio of log-amplitude variances derived from 3D and 2D numerical simulations (+) and analytical (-) as a function of the plane of dimensional reduction defined by α_Z

Results in Polar configuration

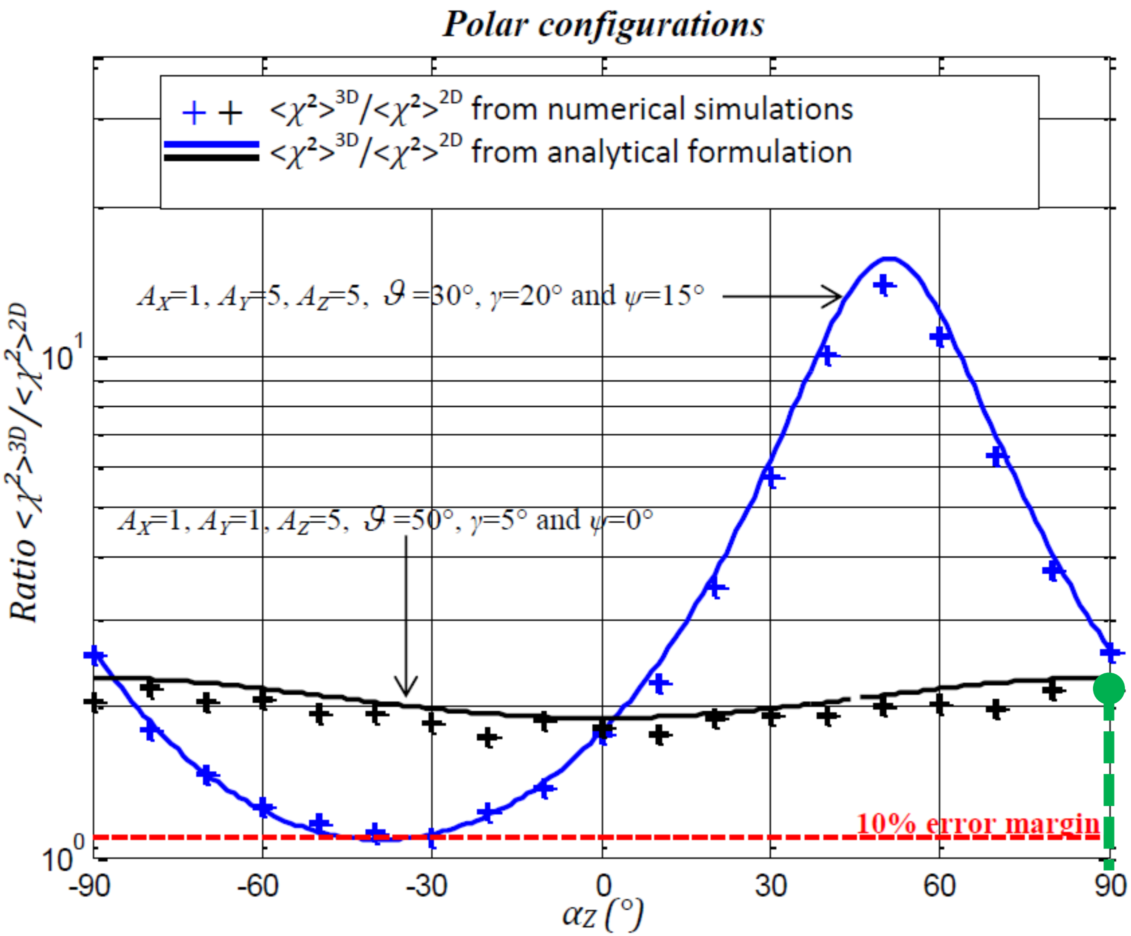

Fig.11: Ratio of log-amplitude variances derived from 3D and 2D numerical simulations (+) and analytical (-) as a function of the plane of dimensional reduction defined by α_Z

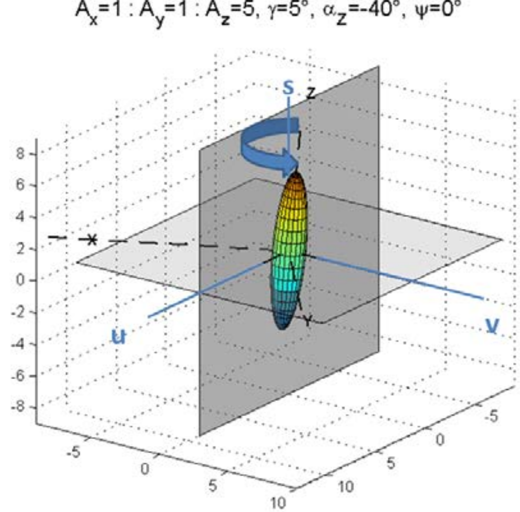

Top View (uOv)

(LOS transverse plane)

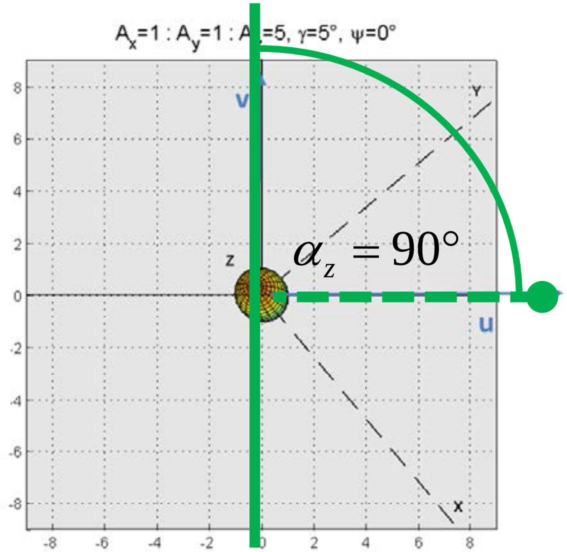

Results in Polar configuration

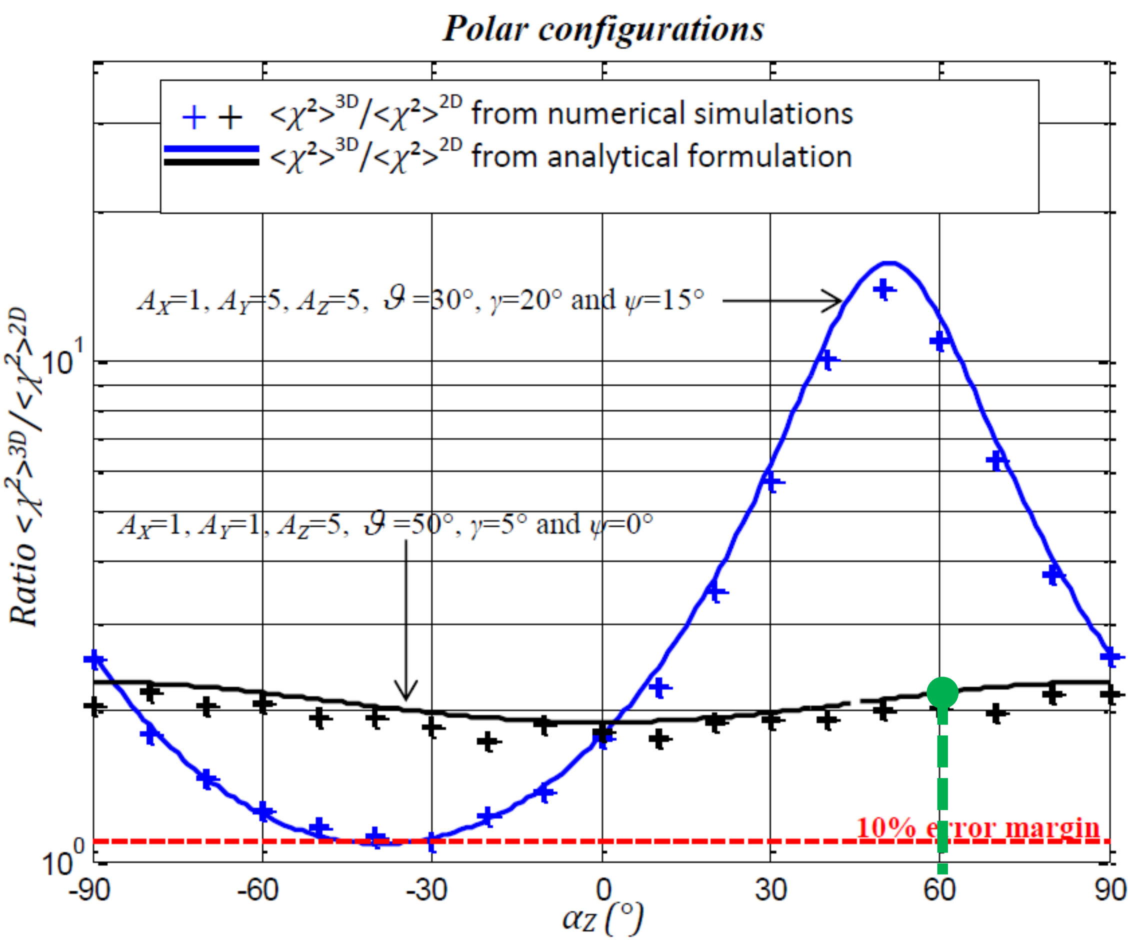

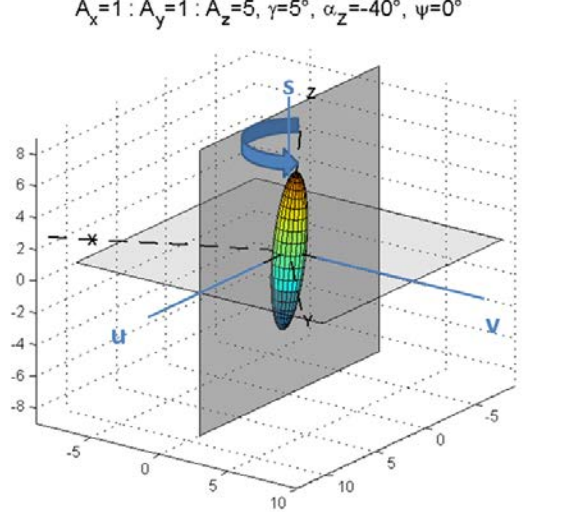

Top View (uOv)

(LOS transverse plane)

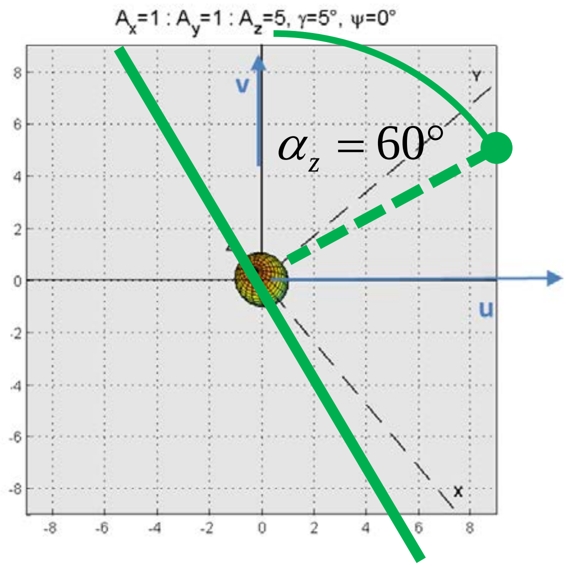

Fig.11: Ratio of log-amplitude variances derived from 3D and 2D numerical simulations (+) and analytical (-) as a function of the plane of dimensional reduction defined by α_Z

Results in Polar configuration

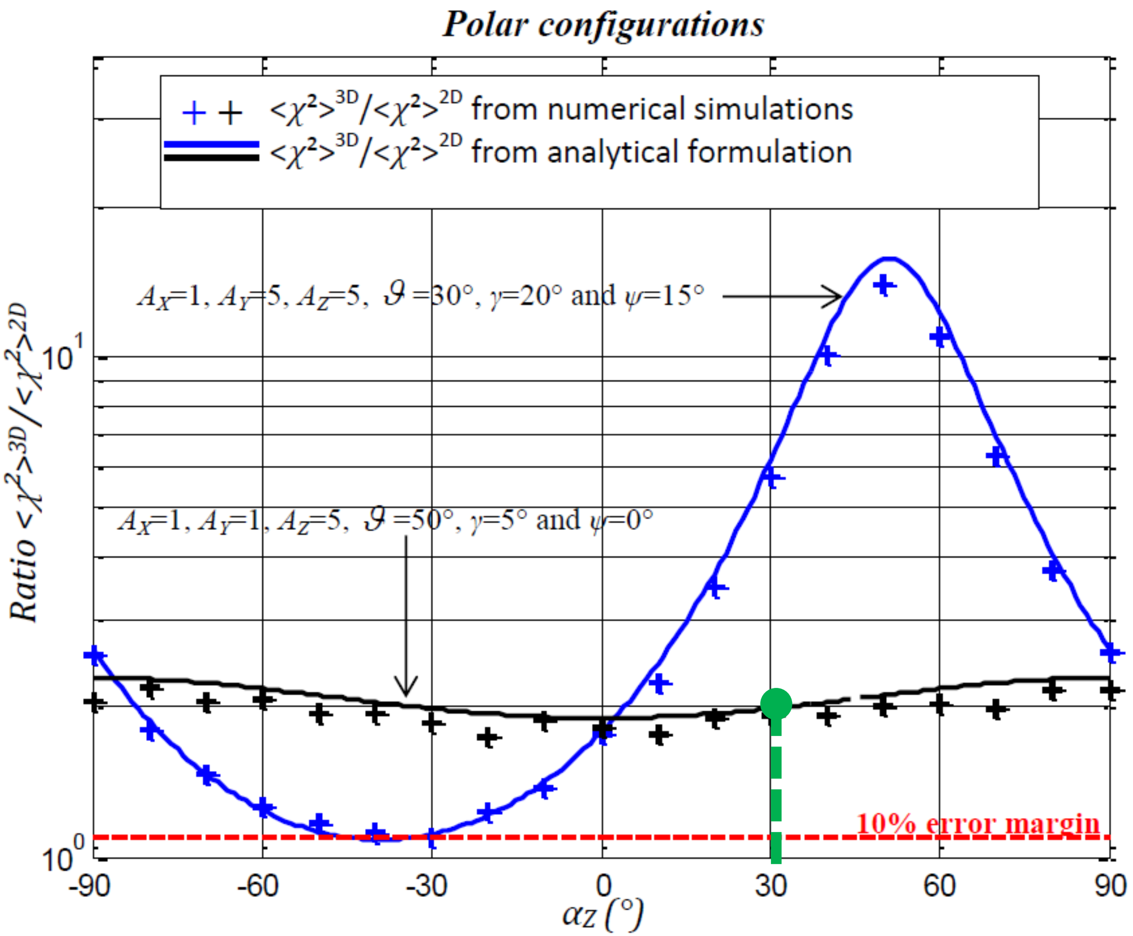

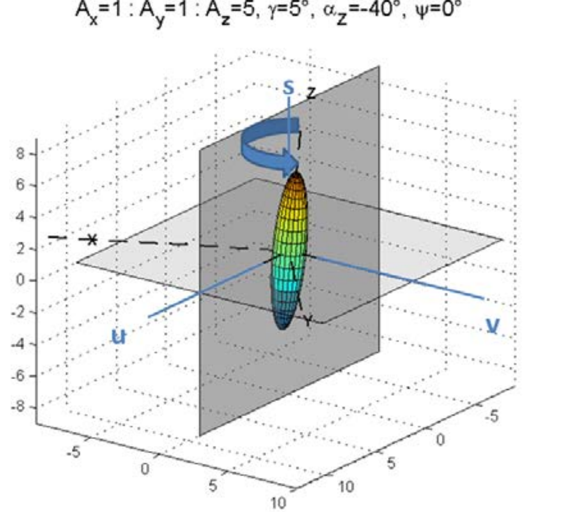

Top View (uOv)
(LOS transverse plane)

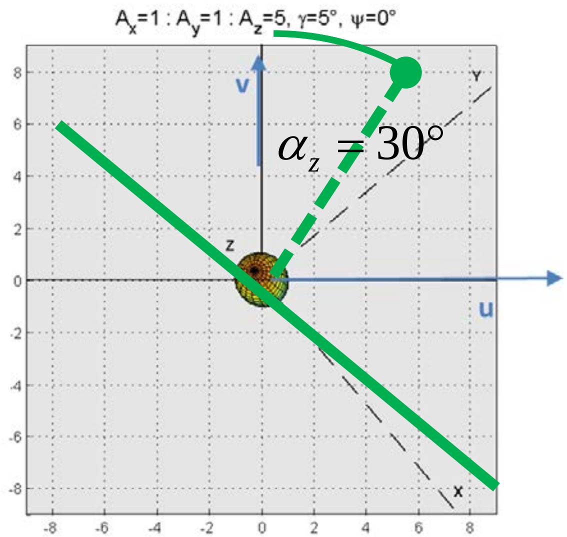

Fig.11: Ratio of log-amplitude variances derived from 3D and 2D numerical simulations (+) and analytical (-) as a function of the plane of dimensional reduction defined by α_Z

Results in Polar configuration

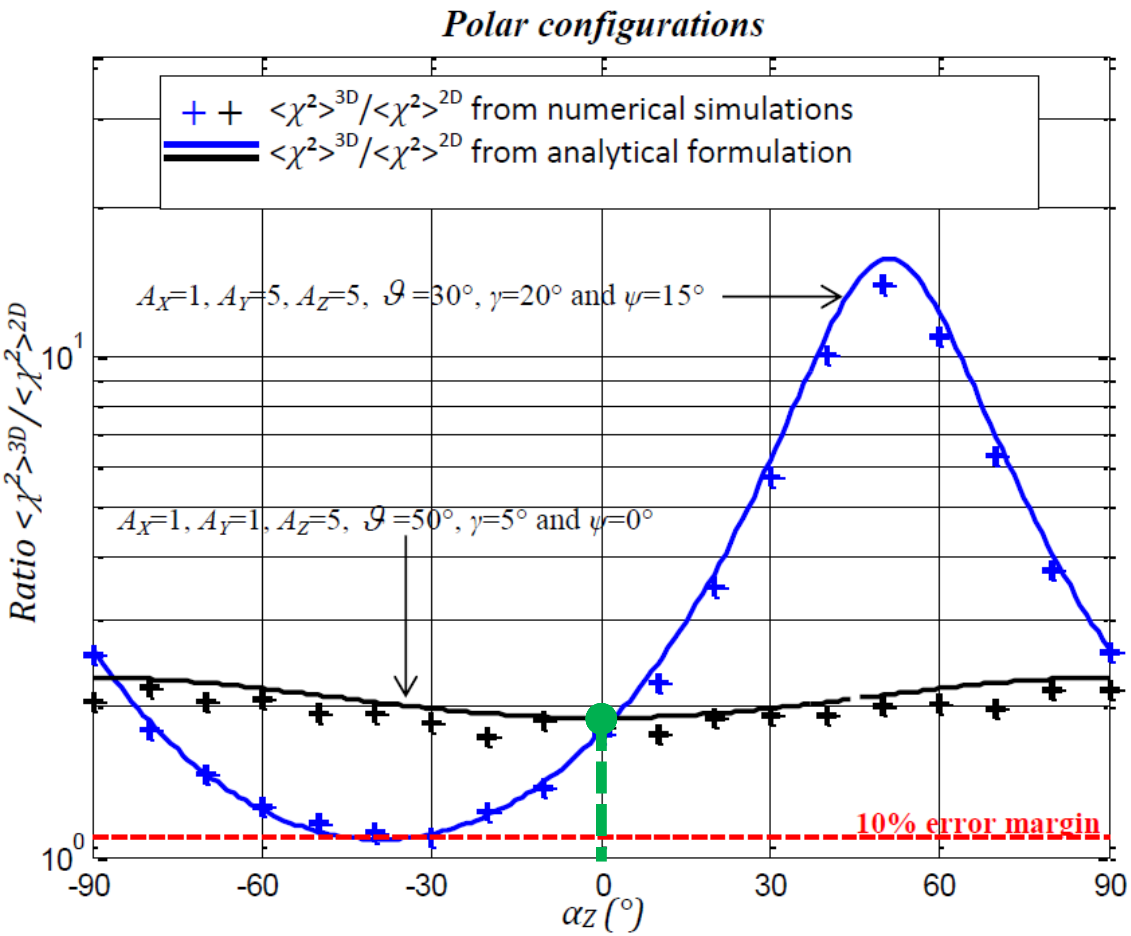

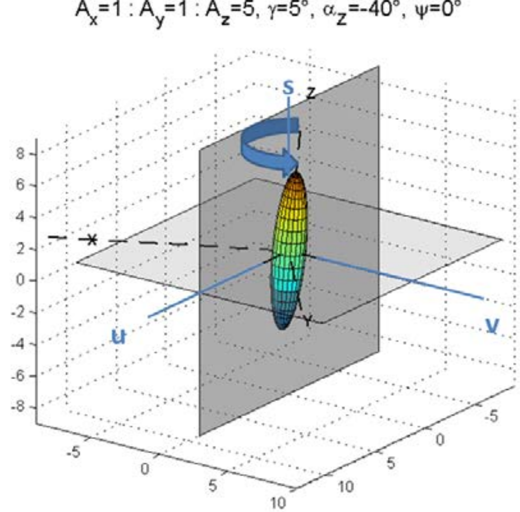

Top View (uOv)
(LOS transverse plane)

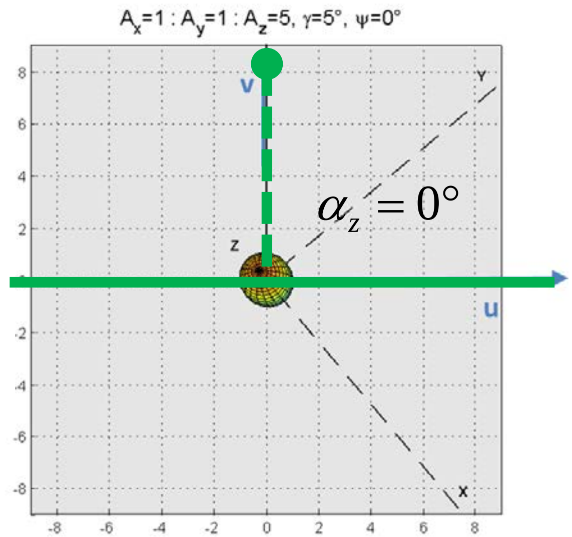

Fig.11: Ratio of log-amplitude variances derived from 3D and 2D numerical simulations (+) and analytical (-) as a function of the plane of dimensional reduction defined by α_Z

Results in Polar configuration

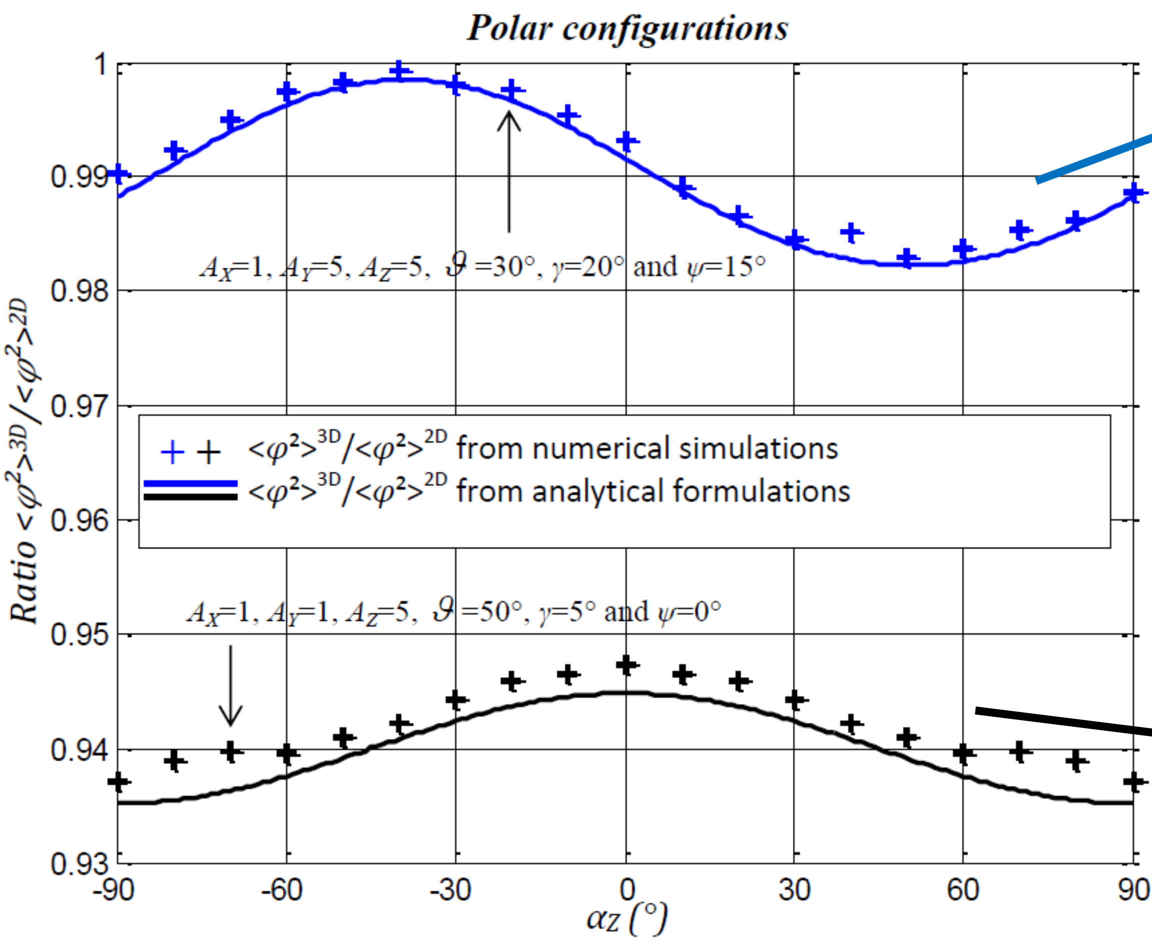

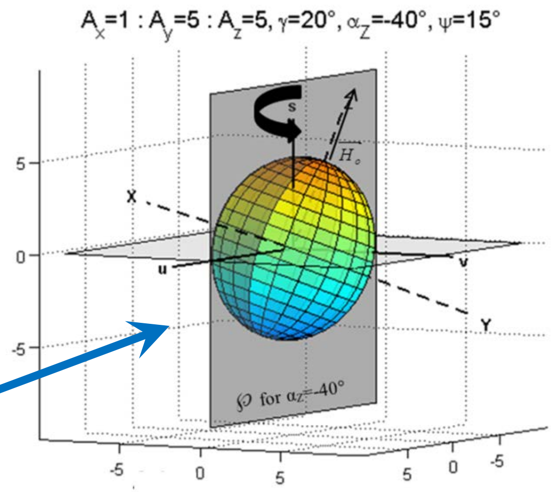

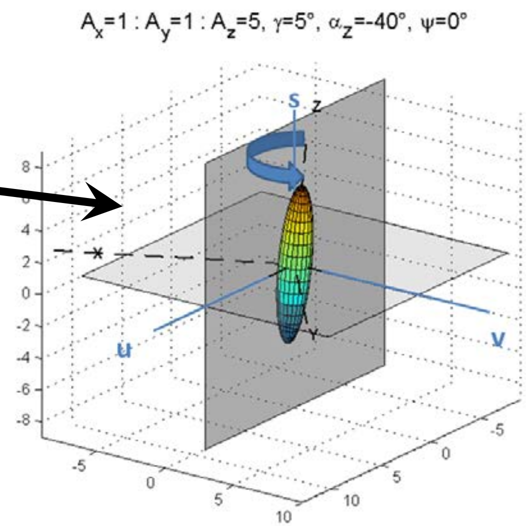

Fig.12: Ratio of phase variances derived from 3D and 2D numerical simulations (+) and analytical (-) as a function of the plane of dimensional reduction defined by α_Z

Conclusion

Study of dimensional reduction 3D to 2D has been performed from numerical (PWE-MPS) and analytical (Rytov) modeling

The results for typical polar and equatorial configurations have shown:

$$\Re_\chi = \frac{<\chi^2>^{3D}}{<\chi^2>^{2D}} \geq 1$$

DR leads to an **underestimation** of the scintillation effects in terms of log-amplitude variances

$$\Re_\varphi = \frac{<\varphi^2>^{3D}}{<\varphi^2>^{2D}} \leq 1$$

DR introduces a **weak overestimation** of the phase variances

From the analytical formulation, these observations **can be generalized**

For more details : « Validity of 2D electromagnetic approaches to predict Log-amplitude and phase variances due to 3D ionospheric scintillation effects", Hélène Galiègue, Laurent Féral, Vincent Fabbro

To be submitted very soon to JGR

Thank you for your attention